Promoting the Clinical Relevance of 3D Bioprinting

Peter Apelgren

Department of Plastic Surgery
Institute of Clinical Sciences at
Sahlgrenska Academy
University of Gothenburg
Gothenburg, Sweden, 2022

UNIVERSITY OF
GOTHENBURG

Cover illustration by Peter Apelgren

Promoting the Clinical Relevance of 3D Bioprinting

peter.apelgren@gu.se

ISBN 978-91-8009-620-1 (print)
ISBN 978-91-8009-621-8 (pdf)

Printed in Borås, Sweden 2021
Printed by Stema Specialtryck AB

"*A mind is like a parachute.*
It doesn't work if it is not open."
Frank Zappa

Table of Contents

I. Abstract

This thesis focuses on the development of methodologies enabling the reconstruction of autologous, functional, and long-term-stable cartilage-like tissue using 3D bioprinting technology and animal experiments. The stability, resilience, and *in vivo* viability of the printed cells and tissue vascularization, as well as the observed immunogenicity and safety, represent the main issues evaluated and discussed in this thesis. Furthermore, the mechanical properties of the applied biomaterials are evaluated in detail.

Study I
Background: This study quantitatively assessed the proliferative capacity of chondrocytes in the presence and absence of stem cells in the 3D bioprinting setting.
Results: We observed significant increases in the number of chondrocytes and cluster formations during the study period. Compared with pure human nasal chondrocyte (hNC) group, we identified a significant additional proliferative effect in the group containing both hNCs and stem cells, and histologic analysis confirmed the expected production of collagen type II in the extracellular matrix, as well as the distribution of glycosaminoglycans in the cartilage-like tissue. Additionally, fluorescence *in situ* hybridization analysis confirmed that the chondrocytes were of human origin, and their male phenotype verified the male chondrocyte-donor source.

Study II
Background: In this study, we evaluated the results of subcutaneous implantation of 3D-bioprinted constructs mixed with human chondrocytes and stem cells over the course of 10 months.
Results: We observed no signs of necrosis, tumors, ossification, or other adverse effects. Moreover, the constructs remained well-preserved, and histologic analyses showed thriving, proliferating chondrocytes in cartilage-like formations.

Study III
Background: This study mapped the vascularization of gridded 3D-bioprinted constructs.

Results: Perfusion data from magnetic resonance imaging revealed progressive vascularization inside of grid holes that were confirmed as being filled with blood vessels connected to host circulation according to histologic analysis. Additionally, immunohistochemical analysis of endothelial cells confirmed the vascular arrangement, with collagen II production further indicating chondrocyte proliferation and cartilage formation.

Study IV
Background: In this study, we evaluated the biocompatibility (according to ISO standards) and mechanical properties of tunicate-derived nanocellulose (TNC) as a novel biomaterial.
Results: We determined TNC biocompatibility as equivalent to that of expanded polytetrafluoroethylene while also exhibiting excellent mechanical properties.

Keywords
3D bioprinting, cartilage, chondrocytes, stem cells, tissue engineering, nanocellulose, hydrogel, bioink, vascularization, biocompatibility

II. Summary in Swedish

Rekonstruktion av förlorade kroppsdelar såsom en näsvinge, ett bröst eller ett ytteröra utgör idag en stor utmaning inom plastikkirurgin. Det funktionella resultatet är alltid högst prioriterat men den kosmetiska dimensionen är också central, särskilt i ansiktet.

Med hjälp av 3D-bioprintingteknologi kan man utifrån patientens egna celler återskapa form och funktion. Patientens celler blandas med en bärargel (”biobläck”) och laddas i en 3D-bioprinter som sedan lager för lager bygger upp en tredimensionell struktur. Strukturen kan sedan transplanteras till önskad plats.

Denna avhandling fokuserar på metodutveckling och utvärdering av 3D-bioprintad human broskvävnad genom främst *in vivo*-studier i nakenmusmodell. Med hjälp av bland annat histologi, immunohistokemi och MRI har biologiska egenskaper hos den 3D bioprintade vävnaden analyserats på cellnivå.

III. List of publications

This thesis is based upon the following papers referred to in the text by their Roman numerals.

I. **Apelgren, P.**, Amoroso, M., Lindahl, A., Brantsing, C., Rotter, N., Gatenholm, P., Kölby, L.
Chondrocytes and Stem Cells in 3D-bioprinted Structures Create Human Cartilage in vivo. *PLoS ONE* **12**, e0189428 (2017).

II. **Apelgren, P.**, Amoroso, M., Säljö, K., Lindahl, A., Brantsing, C., Stridh Orrhult, L., Markstedt, K., Gatenholm, P., Kölby, L.
Long-term in vivo integrity and safety of 3D-bioprinted cartilaginous constructs. *J Biomed Mater Res B Appl Biomater* **109**, 126-136 (2021).

III. **Apelgren, P.**, Amoroso, M., Säljö, K., Montelius, M., Lindahl, A., Stridh Orrhult, L., Gatenholm, P., Kölby, L.
Vascularization of tissue engineered cartilage – sequential in vivo MRI display functional blood circulation. *Biomaterials* **276**, 121002 (2021).

IV. **Apelgren, P.**, Sämfors, S., Säljö, K., Mölne, J., Gatenholm, P., Troedsson, C., Thomson, E.M., Kölby, L.
Biomaterial and biocompatibility evaluation of tunicate nanocellulose for tissue engineering and 3D bioprinting applications. Submitted manuscript.

In addition to papers **I–IV** included in this thesis, inspiration and scientific experience were obtained from three complementary publications (referred to by in-text citations):

- **Apelgren, P.**, Amoroso, M., Säljö, K., Lindahl, A., Brantsing, C., Stridh Orrhult, L., Gatenholm, P., Kölby, L. Skin Grafting on 3D Bioprinted Cartilage Constructs In Vivo. *Plast Reconstr Surg Glob Open* **6**, e1930 (2018). https://doi.org/10.1097/GOX.0000000000001930

- **Apelgren, P.**, Karabulut, E., Amoroso, M., Mantas, A., Martínez Ávila, H., Kölby, L., Kondo, T., Toriz, G., Gatenholm. P. In vivo human cartilage formation in 3D bioprinted constructs with a novel bacterial nanocellulose bioink. *ACS Biomater. Sci. Eng*. 2019; **5** (5) (2019). https://doi.org/10.1021/acsbiomaterials.9b00157

- Amoroso, M., **Apelgren, P.**, Säljö, K., Montelius, M., Strid Orrhult, L., Engström, M., Gatenholm, P., Kölby, L. Functional and morphological studies of in vivo vascularization of 3D-bioprinted human fat grafts. *Bioprinting*. 2021; 23, e00162 (2021). https://doi.org/10.1016/j.bprint.2021.e00162

IV. Abbreviations

ABvG	Alcian Blue van Gieson staining
ASC	Adipose stem cell
AT	Arrival time
BALB/C	Laboratory-bred strain of the house mouse (the name is a concatenation of founder Halsey J. Bagg and albino)
BMP	Bone morphogenetic protein
BNC	Bacterial nanocellulose
ColX	Collagen type X
DCE	Dynamic contrast-enhanced imaging
DMEM	Dulbecco's modified Eagle medium
DWI	Diffusion-weighted imaging
ECM	Extracellular matrix
ePTFE	Expanded polytetrafluoroethylene
FDA	Food and Drug Administration
FGF	Fibroblast growth factor
FISH	Fluorescent *in situ* hybridization
FBS	Fetal bovine serum
GAG	Glycosaminoglycan
hBM-MSC	Human bone marrow-derived mesenchymal stem cell
hNC	Human nasal chondrocyte
IGF	Insulin-like growth factor
iPSC	Induced pluripotent stem cell
IS	Initial slope
ISO	International organization for standardization
MRI	Magnetic resonance imaging
MSC	Mesenchymal stem cell
NC	Nanocellulose
NFC	Nanofibrillated cellulose
OA	Osteoarthritis
PBS	Phosphate-buffered saline
PCL	Poly-ε-caprolactone
PTH1R	Parathyroid hormone 1 receptor

PTHrP	Parathyroid receptor-like protein
RUNX	Runt-related transcription factor
SOX9	Sex-determining region Y (SRY)-box 9
SVF	Stromal vascular fraction
TGF	Transforming growth factor
TNC	Tunicate-derived nanocellulose

V. Definitions

Angiogenesis	Development of new blood vessels
Anotia	Congenital deficiency of the outer ear
Alginate	A seaweed-derived polysaccharide
Arrival time (AT)	The time for MR signal amplitude to increase above baseline levels. A short AT reflects an early arrival of the contrast agent.
Bioink	A printable cell-supporting material
Cell-laden	In this context, biomaterials loaded with cells
Chondrocyte clustering	Three or more chondrocytes within a cartilage cavity (i.e., lacunar space)
Chondron	A chondrocyte and its immediate surroundings (pericellular matrix and pericellular capsule)
Endochondral pathway	One of two possible pathways towards tissue ossification (the transformation of cartilaginous tissue into bone)
Exosome	An extracellular vesicle that stores and transports DNA, RNA, and signaling proteins
Extracellular matrix (ECM)	Connective tissue outside of cells and that also contains supporting and anchoring structures that play critical roles in tissue-specific cell dynamics and signaling
Extraterritorial matrix	Connective tissue outside of close proximity to a cell (i.e., territorial matrix)
Glycosaminoglycans (GAGs)	Negatively-charged polysaccharide compounds ubiquitous in mammalian tissues

Hyaluronan	A large and highly water-absorbing GAG connecting other GAGs and forming a proteoglycan
Initial slope (IS)	The rate at which contrast enters the interstitial space (high IS indicates high tissue perfusion)
Microtia	Congenital deformation of the outer ear
Nanocellulose (NC)	Nanostructured cellulose produced by bacteria or derived from plants and tunicates
Ossification	Transformation of cartilage into bone (i.e., endochondral ossification) or direct bone formation in connective tissue (i.e., intramembranous ossification)
Proteoglycans	Proteins comprising a core protein and covalently-attached GAGs and prevalent in connective tissues and the ECM in cartilage
Territorial matrix	Proteoglycan-rich ECM in close proximity to a chondrocyte
Vasculogenesis	The process of precursor cells differentiating into endothelial cells during vessel formation
Voxel	A volume pixel

1. Introduction

1.1 The evolution of 3D bioprinting technology

3D bioprinting technology originates from the invention of stereolithography in the 1980s (*1, 2*), where a photosensitive polymer could be solidified layer-by-layer using, for example, ultraviolet light. In 1989, Forgacs et al. (*3*) published the first study exploring its possible application in tissue engineering by growing cells in a spatial scaffold. In 1999, researchers at Wake Forest University School of Medicine built a synthetic urinary bladder, where autologous urothelial cells were seeded onto a 3D-printed collagen structure and then transplanted into a patient (*4*). The first bioprinter was created from a modified inkjet printer in the early 2000s (*5*), with further improvements realized in subsequent years through biomaterial research resulting in the development of viscous biological inks (i.e., "bioinks") enabling arrangements in three dimensions. The first commercial bioprinter was introduced in 2009 (NovoGen MMX; Organovo, San Diego, CA, USA) and from which multiple types of bioprinting techniques have evolved.

1.2 Clinical applications of 3D bioprinting technology

The goal for tissue engineering and 3D bioprinting is to create functional, autologous solid organs. In theory, the 3D bioprinter is unlimited in regard to the cell types or tissue architecture for which it can be programmed to construct; however, there are numerous biological limitations that have been addressed over the previous 20 years.

Most cartilage-specific research related to tissue engineering has focused on orthopedics and, more specifically, the relief of osteoarthritis (OA), which presents an enormous need for new treatment methods. For example, osteoarthritic joints lacking pressure-absorbing cartilage affect ~600 million individuals (6). Using the new technologies offered by tissue engineering and 3D bioprinting,

orthopedic researchers have developed and evaluated multiple methods.

In 1994, Brittberg et al. (*7, 8*) demonstrated a method to transplant chondrocytes into focal cartilage defects in joints (a method later termed autologous chondrocyte implantation) and commercialized as the Carticel method (Genzyme Biosurgery, Cambridge, MA, USA). This method is still successfully used and represents a reliable alternative to other orthopedic methods (e.g., microfracturing of the subchondral bone that results in bone marrow stimulation and stem cell access to the injury site) (*9*). Additionally, Jiang et al. (*10*) described a reconstruction method using chondrocyte-progenitor cells for efficient cartilage regeneration of articular osteochondral defects. Moreover, a recent study reported testing of a more complex procedure involving surgical replacement of a damaged meniscus with 3D-bioprinted substitutes (*11*).

In spinal surgery, different fusion procedures represent the gold standard for treating degenerative disc disease (*12*); however, in some cases, patients would possibly benefit from a disc replacement. Several different biomaterials [e.g., hydrogels (*13, 14*) and cell therapies (e.g., chondrocytes (*15, 16*) or mesenchymal stem cells (MSCs) (*17, 18*)] have been proposed, where 3D bioprinting technology can customize a replacement disc. A recent study by Wu et al. (*19*) described 3D bioprinting of a cell-laden polymer–hydrogel intervertebral disc, followed by its surgical implantation to replace native discs in rats. Their findings showed that the cell-laden discs maintained height and promoted the deposition of collagen and proteoglycans.

3D bioprinting technology has expanded to applications in almost any field of medicine, including 3D-bioprinted replacement patches for damaged myocardium (*20*), autologous heart valves (*21*), and retinal reconstruction (*22*). Rapidly evolving engineering techniques and continued biological research will likely enable reconstruction of even more complex tissues using 3D bioprinting. Although complex shapes and composite cell layers can now be easily fabricated, printing resolution remains a determining factor in their utility. For example, the microarchitecture of liver tissue is extremely intricate and requires high printing resolution, as well as perfectly accurate cellularity. Additionally, multipurpose, metabolically hyperactive

hepatocytes are dependent upon efficient and direct blood perfusion. To push the resolution limits, novel and efficacious approaches to functionalize intricate micro-/nanofibrous scaffolds of liver lobuli have been developed (*23, 24*).

1.3 Potential applications of 3D bioprinting in reconstructive plastic surgery

In reconstructive plastic surgery, the application scope of 3D bioprinting technology is substantial, and restoration of damaged or malformed cartilaginous features represents an important commitment for the plastic surgeon. Traumatic injuries or congenital malformations of composite cartilaginous structures (e.g., nose and/or auricle) are common challenges in plastic surgery. In some cases, the entire structure is distorted, whereas in others, subunits are lost or damaged. To treat these patients, current methods include different techniques to replace or reshape using tissue from another part of the patient or synthetic implants. However, all of these methods have drawbacks related to either the donor site or associated with implanted foreign materials.

To reconstruct facial cartilaginous structures using autologous tissue, cartilage is typically harvested from the auricular conchae (*25, 26*), costochondral joints (*27-29*), or septum nasi (*30, 31*). Harvesting procedures from the concha can cause donor-site infections and cosmetically unfavorable scarring, whereas harvesting from the rib cage often causes pain and long-term disfigurement (*32-34*). Using costochondral cartilage for auricular reconstruction represents the current gold standard (Figure 1A and B); however, these procedures are surgically challenging, multi-staged, time-consuming, and the long-term results are difficult to predict.

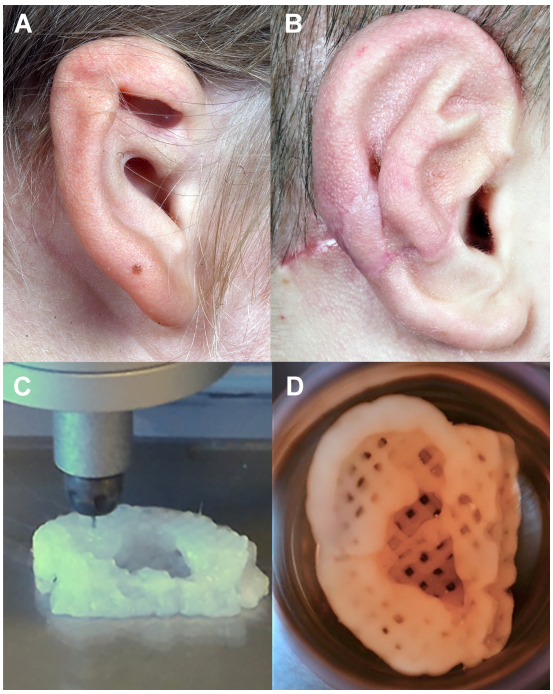

Figure 1. Microtia. Concha-type microtia grade II and ear-canal atresia (A). Two months after the final operation in the two-staged ear-reconstruction procedure *ad modum* Firmin (*35*) using costochondral cartilage as a scaffold (B). 3D bioprinting of a scaffold for auricular reconstruction (C and D).

Another approach to addressing auricular malformations involves the use of different kinds of synthetic prosthetics, which gained recognition with the introduction of osseointegrated (bone-anchored) titanium fixtures in the early 1980s (*36*). These procedures are typically a secondary choice in the presence of contraindications to an autologous reconstruction (*37*). Complications include local soft-tissue reactions and infection (*38*) and failure of the bone-anchoring fixtures (*39*). Furthermore, these methods require two operations. Additionally, although the bone fixtures usually last a lifetime, the prostheses must be replaced every 2 to 5 years (*40*).

3D bioprinting technology can potentially omit some of the complicating factors related to these methods and supply the reconstructive surgeon with additional possibilities. First, the required autologous cells can be more conveniently harvested, as instead of surgical excision of cartilage, chondrocytes can be retrieved from small biopsies of the nasal septum under local anesthesia in an outpatient setting and without major donor-site morbidity. However,

the chondrocytes must be seeded and expanded *in vitro*, which adds both biological and regulatory convolutions. Second, the delicate and complex shapes of the tissue (e.g., an auricle) can easily be reproduced with high resolution using a 3D bioprinter rendering a mirrored blueprint of the contralateral ear (Figure 1C and D). The autologous cells are then processed and arranged in a predetermined and precise 3D pattern that mimics the lost or damaged body part perfectly. Third, contrary to synthetic materials and prosthetics, the grafts can be transplanted without any graft-rejection issues. Fourth, after the outpatient harvesting procedure and laboratory expansion, some reconstructions can potentially be completed in one surgical session.

Beyond cartilaginous tissues, there exist other clinical challenges where 3D bioprinting technology and tissue engineering can expand treatment options in plastic reconstructive surgery, including mandibular bone destruction related to irradiation treatment (i.e., osteoradionecrosis) and breast reconstructions after mammary cancer. Notably, 3D-printed synthetic, provisional bone replacements have been used clinically for decades in maxillofacial surgery to bridge the time gap until definitive reconstruction. Recently, several different tissue-engineering approaches have been proposed as a permanent solution that omits the need for a provisional scaffold or even sparing patients major surgical interventions altogether. For example, injection of stem cells has been evaluated as a more moderate approach to alleviating pain relative to surgery (*41*). Moreover, custom-made, autologous, 3D-bioprinted osseous mandible replacements represent a potential alternative approach through the use of electrospinning technology and converged biofabrication (*42*). Furthermore, although microsurgical anastomoses will still be necessary, the complicated harvesting procedures and the associated donor-site morbidities related to free fibula grafts can be avoided.

For breast-reconstructive purposes, 3D-bioprinted autologous adipose tissue that perfectly mimics the contralateral breast can potentially become a reality within the next decade. Pati et al. (*43*) encapsulated adipocyte stem cells in a composite bioink comprising poly-ε-caprolactone (PCL) and decellularized adipose tissue. After 14 days *in vivo* (following subcutaneous injection into nude mice), they observed that the constructs maintained their 3D shape, volume,

and high cell viability, as well as displayed potent adipogenesis and angiogenesis. Additionally, Cho et al. (*44*) used extrusion bioprinting to print bioink comprising preadipocytes and human umbilical vein endothelial cells along with a scaffold of decellularized extracellular matrix (ECM) and PCL that resulted in enhanced adipogenesis and neovascularization. Moreover, our research group has conducted two *in vivo* experiments with adipose tissue (*45, 46*). Briefly, implantation of 3D-bioprinted lipoaspirate constructs in nude mice without any prior expansion or *in vitro* cultivation resulted in functional vascularization after 60 days *in vivo* along with adipose tissue survival in the absence of necrosis.

Reconstructions after burn traumas frequently involve skin grafts to replace lost skin areas. Skin transplants usually lead to scarring, long-term disfigurement, and decreased functionality (e.g., lost elasticity). Skin biopsies (punch grafts; regarded as small, full-thickness grafts) have been used for wound healing for several decades, with the grafts applied at the wound site eventually able to regenerate skin tissue. This method is mainly used to treat recalcitrant wounds (*47*). However, due to skin-graft shortages and the inability of some patients to heal from additional wounding, some large areas cannot be amended in this manner. Furthermore, the morbidity caused by scarring often remains. Others have further developed the punch-graft method to regenerate skin using seeded keratinocytes complemented with a biodegradable carrier matrix, which has resulted in a thicker neoepidermis (*48*).

In the search for other alternatives, different tissue-engineering techniques have been evaluated, including the use of functionalized biomaterials that allow accelerated healing and reduced scarring in addition to the exclusion of donor-site wound areas (*49*). Clinically available examples include bilayered composite dermal substitutes (e.g., Integra) (*50, 51*) and polyglactin meshes encompassing human fibroblasts (e.g., Dermagraft) (*52*).

Furthermore, methods for skin regeneration involving 3D bioprinting have emerged and expanded the clinical options for managing different skin wounds. Similar to the described tissue-engineered methods, a 3D bioprinter enables functionalization of different biomaterials (e.g., the addition of cells and/or growth factors) and facilitates customization of wound dressings to perfectly

fill the wound cavity, thereby allowing for enhanced cell–cell contact, surface attachment, and diffusion of oxygen and nutrients. Many promising results have been reported. An excellent review by Weng et al. (*53*) summarizes the current status of 3D bioprinting of skin.

1.4 Clinical translation

The following constitute obstacles to clinical translation of 3D bioprinting technology for cartilaginous tissues.

1. Chondrocytes have to survive the bioprinting procedure.
2. Chondrocytes have to be able to proliferate and eventually create novel cartilage-like tissue.
3. The long-term resilience and shape-stability of the 3D-bioprinted structures must be assured.
4. Safety-related concerns must be appraised.
5. Biocompatibility and biomechanical properties of the scaffolding bioink must be evaluated.
6. The biomaterial must be permeable to allow for the diffusion of oxygen and nutrients.
7. The 3D-bioprinted cartilage-like structures should be able to convey vascularization to provide other tissues (e.g., a skin graft) with oxygen and nutrients.
8. The minimally-invasive harvesting procedure yields only a small number of cells, and the chondrocytes would need to be cultured and expanded before bioprinting. This adds an extra dimension to logistics, lab resources, and legislative oversight.

This thesis focuses mainly on addressing the issues described in 1 through 7 and provides a scientific foundation for the translation to further clinical studies.

1.5 Chondrocytes and cartilage

Chondrocytes

Chondrocytes constitute 2% to 10% of the total cartilage volume, with ~90 chondrocytes/mm^2 present in histological sections of articular cartilage (*54, 55*). The healthy chondrocyte is morphologically round, ovoid, or increasingly discoid near tissue boundaries, with a diameter between 10 µm and 30 µm (*56*), and displays a distinct nucleus. The cell, including its immediate surroundings (pericellular matrix and pericellular capsule), is termed a chondron (Figure 2). The pericellular matrix contains aggrecan, glycosaminoglycans (GAGs), and collagen. Proliferating chondrocytes and chondrocyte clusters arising from mitosis form isogenous (clonal) groups (i.e., cell nests) that typically reside in lacunae. The near surroundings of a lacuna (i.e., the territorial matrix) contain mainly negatively-charged proteoglycans, resulting in a highly basophilic micro-milieu. Chondrocytes natively prefer to aggregate on surfaces and are highly dependent on a semi-enclosed and stable micro-milieu.

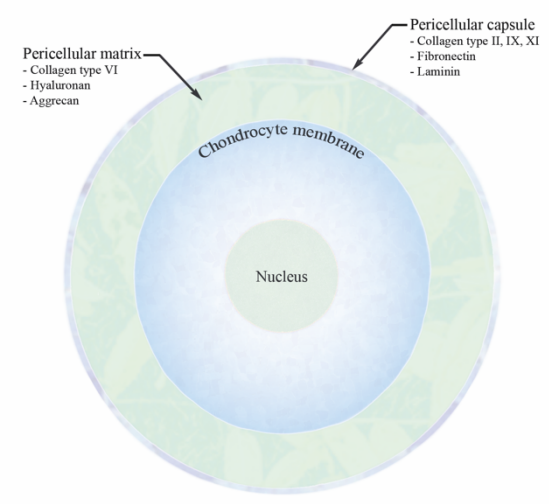

Figure 2. The chondron–chondrocyte microenvironment. The surrounding pericellular matrix and capsule contain different collagen subtypes, GAGs, and proteoglycans that create a protective barrier for the chondrocyte. The pericellular matrix, pericellular capsule, and the chondrocyte itself make up a chondron. Adapted from Gahunia et al. (*57*).

Chondrocytes natively differentiate from MSCs in a process initiated by paracrine stimuli, induction of key transcription factors, and activation of chondrocyte-specific genes (*58*) and continues through cell proliferation and secretion of cartilage-specific ECM

proteins mainly comprising type II collagen and aggrecan (*59*). Sex-determining region Y (SRY)-box 9 (SOX9) is among the most important signaling molecules in this process and represents a transcriptional factor essential for the differentiation of mesenchymal cells towards the chondrocyte phenotype (Figure 3). SOX9 upregulates fundamental chondrogenic genes, including c*ollagen type II alpha 1 chain* and *ACAN* (encoding aggrecan) (*60, 61*), represses hypertrophy and bone transformation by blocking *Runt-related transcription factor 2* (*RUNX2*) expression (*62*), and is regulated by other SOX family transcription factors (i.e., SOX5 and SOX6) (*63*). The chondrogenic differentiation of MSCs is also regulated by bone morphogenetic protein-4 (BMP-4) and fibroblast growth factor (FGF) receptor 2 (*64, 65*), which in turn induces upregulation of SOX9 levels (*66*). The proliferation of mature chondrocytes is regulated by transforming growth factor (TGF)-β, FGF1 (*67*), and insulin-like growth factor (IGF)-1 (*68*).

Mature chondrocytes are prevented from hypertrophy and further differentiation along the endochondral pathway (i.e., ossification) mainly by negative feedback from SOX9 and parathyroid hormone-related peptide (PTHrP). RUNX transcription factors (e.g., RUNX2 and RUNX3) promote chondrocyte hypertrophy transformation and osteoblast formation through the expression of type X collagen (ColX), matrix metalloproteinases, and Vascular endothelial growth factor (*69*). RUNX2 and RUNX3 are suppressed by SOX9 and PTHrP.

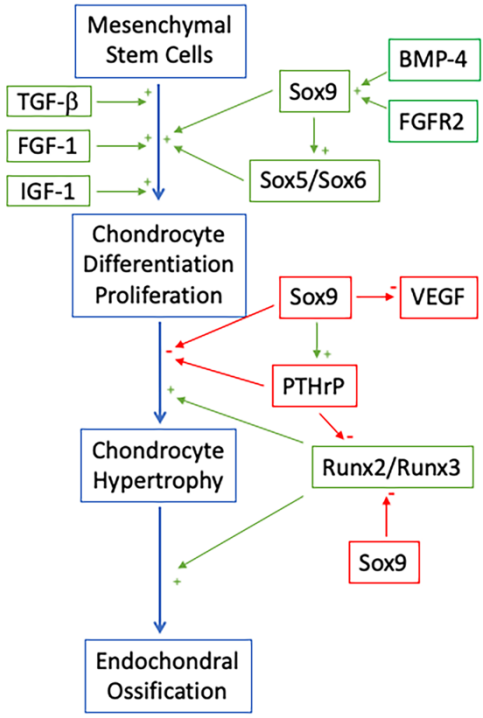

Figure 3. Chondrocyte differentiation and proliferation. The SOX9 transcription factor promotes differentiation from MSCs towards a chondrogenic phenotype. TGF-β and IGF-1 promote chondrocyte proliferation, and SOX9 suppresses mature chondrocytes from further transformation along the endochondral pathway. Adapted from Nishimura et al. (*70*).

In addition to the MSC-differentiation process, immature chondrocytes start producing ECM constituents (e.g., collagen proteins and proteoglycans). Eventually, chondrocytes arrange in lacunae, where isogenous groups cluster and form cartilaginous tissue (Figure 4).

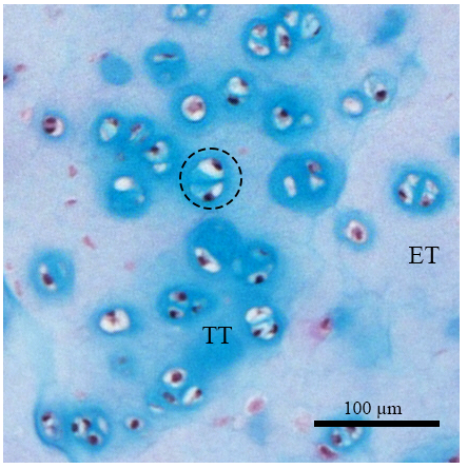

Figure 4. A 3D-bioprinted cartilage-like implant. The constructs, comprising bacterial nanocellulose and human nasal chondrocytes, were subcutaneously implanted in a nude mouse model. After 60 days *in vivo*, thriving chondrocytes were observed. The isogenous groups (circled) gather in clusters, and GAGs produced by the proliferating chondrocytes are excreted to the territorial matrix (TT), visualized in blue using Alcian Blue van Gieson staining. The extraterritorial matrix (ET) displays less staining intensity. Bar = 100 µm. The image was cropped and adjusted for contrast and exposure. Previously unpublished image from (*71*).

Cartilage

Mesenchymal tissues found in the head and neck region originate from the ectoderm and differentiate from neural crest cells at the pharyngeal arches to form cartilage composite features, such as the auricle. All other cartilaginous tissue and bone structures in the human body derive from the mesoderm. A recent study outlined some biological differences in both function and activity depending on which germ layer the chondrocytes used for regenerative purposes are derived (*72*).

Cartilaginous tissues lack vascularization, innervation, and lymphatic drainage, whereas chondrocytes thrive on diffusion in a low-oxygen-tension micro-milieu. The cell metabolism in articular cartilage is adapted to an oxygen tension varying from 9% to 2% O_2 in synovial fluid (*73, 74*), and cell survival, as well as GAG and type II collagen synthesis, is improved under such low-oxygen-tension conditions (*75-77*). Furthermore, chondro-inductive genes are suppressed by high O_2 tension (*78, 79*).

Cartilage is a versatile connective tissue widely distributed in the human body and comprises three different conformations.

- Hyaline cartilage is found mainly in weight-bearing joints and comprises up to 80% water, relatively few chondrocytes,

and thin fibrils of type II collagen. This cartilage displays high tensile strength and resiliency and is derived from the mesodermal germ layer.
- Fibrous cartilage is found in intervertebral discs and comprises thicker fibers of type II collagen and a higher amount of type I collagen.
- Elastic cartilage, derived from the ectodermal germ layer, has a higher density of chondrocytes and additional fibers made of elastin and is found in the auricle, eustachian tube, and epiglottis.

The multipurpose features of cartilaginous tissue constitute crucial functionality in the human body, including pressure-absorbing capacity and shape stability. Additionally, elastic cartilage supports functionally and esthetically important features through its compliance to bending. However, because cartilage lacks blood vessels and nerves, traumatized cartilage cannot heal but instead restores with fibrosis and permanent shape deformities, as well as loss of its special features, including elasticity.

Importance of the in-between

ECM constituents in cartilage are excreted by chondrocytes and comprise a mixture of growth factors, building blocks, and nutrients that serve as an enclosed nano-milieu that promotes cell regeneration. The ECM constitutes 20% to 40% of the total cartilage volume, and ~90% of cartilaginous ECM comprises type II collagen, with the remaining 10% as proteoglycans (*80*). Additionally, ECM staining reveals a higher proportion of proteoglycans than the territorial matrix. To optimize reconstructive efforts in cartilage 3D bioprinting, attention to ultrastructure (e.g., pore size) and ensuring appropriate cellularity to promote cell interactions in the ECM are paramount (*81*). Aggrecan, the largest proteoglycan in cartilage ECM, comprises chains of GAGs, which are negatively-charged polysaccharide compounds. The most important GAGs in cartilage ECM are hyaluronic acid, chondroitin, and keratin. Hyaluronic acid forms with aggrecans via link proteins to provide osmotic properties critical for pressure absorption. Additionally, chondroitin stimulates type II collagen and proteoglycan production (Figure 5), and

chondronectin, another important ECM protein, connects chondrocytes to type II collagen to stabilize the cartilage micro-milieu.

The importance of the ECM in cartilage regeneration has been further highlighted by results from the use of decellularized ECM, which removes all immunogenic factors while maintaining the architectural properties. For example, in the absence of additional cells, decellularized ECM reportedly improved cartilage regeneration in osteochondral defects in rabbits (*82*).

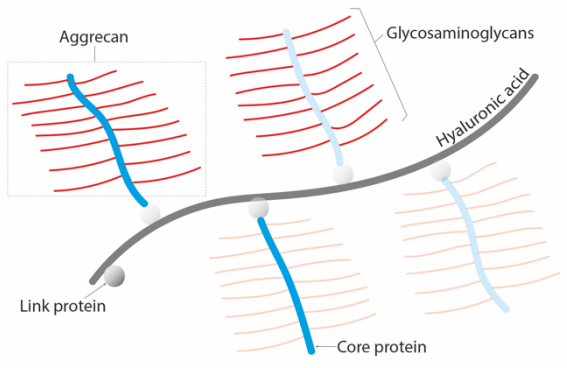

Figure 5. The proteoglycan polymer. Aggrecan comprises many GAGs. The aggrecan units are linked together by hyaluronan.

Perichondrium

The perichondrium is a well-vascularized connective tissue that surrounds cartilaginous tissue and provides the deeper layers of cartilage with oxygen and nutrients while also secreting matrix components. The perichondrium comprises mainly type I collagen fibers, progenitor cells, and chondroblasts. In joints, synovial fluid replaces the functions of the perichondrium.

Hypertrophy

Development of cartilage into axial bone can be initiated through vascular infiltration of cartilaginous tissue and mechanical factors and is associated with the endochondral ossification pathway. Initiation of the pathway is identified by *PTH1R* and *Indian hedgehog* and morphologically by cell hypertrophy, increased production of ColX, and mineralization. Subsequently, osteoblasts and endothelial cells invade the matrix and replace the cartilage with bone.

Vascularization
Although cartilage is avascular, it must be capable of supporting other tissues in composite organs. For example, adipose tissue and skin have higher demands for direct blood perfusion. Therefore, the underlying cartilage must initially be able to supply sufficient oxygen and nutrients via diffusion. Subsequently, as neovascularization develops, the cartilage must be able to convey the arising capillaries and support their reaching the target tissue.

1.6 Cell sources

Differentiated chondrocytes
There is a relative shortage of easily accessible, autologous chondrocytes. The involvement of laboratory culture and expansion represents a complicated extra step, as well as a potential regulatory hurdle. To address the chondrocyte shortage, researchers have instead utilized more easily accessible and abundant stem cells.

Multipotent stem cells can differentiate into many different cell types depending on the influence of the surrounding micro-milieu. Exposure and proximity to mature chondrocytes initiate stem cell differentiation towards the chondrogenic pathway through paracrine signaling (*83*). Therefore, co-cultivation with cell–cell contact between chondrocytes and stem cells provides a favorable environment for chondrogenesis and subsequently the most often-used approach (*84, 85*). Scaffold-based 3D cultures or scaffold-free 3D microtissues imitate the native cell environment better than traditional cell culture methods and thereby increase functionality and cell viability through enhanced intercellular interaction (*86*). Using a spheroid-culture method, De Moor et al. (*87*) showed improved chondrocyte function (e.g., increased GAG and type II collagen production) as compared with 2D expansion.

Human bone marrow-derived (hBM)-MSCs
Given the proper environmental factors, multipotent BM-MSCs can differentiate into chondrocytes. The advantages of BM-MSCs include their easy isolation, high differentiation potency, low immunogenicity, and that they rarely transform into tumors (e.g., teratomas) (*88*). Additionally, they require less *in vitro* manipulation relative to induced pluripotent stem cells (iPSCs) and embryonic

stem cells. Therefore, hBM-MSCs have been among the most widely used lineages in 3D bioprinting of cartilage-like tissue in the previous decade.

A previous study showed that the presence of mature chondrocytes drives BM-MSC differentiation towards chondrogenesis, with the most efficient BM-MSC:chondrocyte ratio suggested at 4:1 (80% and 20%, respectively) (*67*). Interestingly, a recent study evaluated the ability of BM-MSCs to diminish inflammation by downregulating cytokine-related effects associated with SARS-COV-2-infection (*89*). However, limitations to their use include the required invasive harvesting procedures, as well as age-related decreases in cellular function and declining differentiation capacity after serial cultivations (*90-92*).

iPSCs

iPSCs are obtained from genetically reprogrammed adult somatic cells (e.g., fibroblasts) that can be directed down the mesenchymal cell pathway. In addition to preserving the advantages of BM-MSCs, iPSCs also exhibit a higher proliferative capacity (*93, 94*). Interestingly, iPSCs can be programmed using gene editing to generate more inflammation-resistant cartilage (*95*). Furthermore, iPSCs have advantages over embryonic stem cells, which pose considerable ethical issues (*96*). However, compared with BM-MSCs, iPSCs pose a higher risk of teratoma formation, which limits their clinical translation (*97, 98*), although this risk can potentially be mitigated by chemical alterations (*99*).

Other cell sources

PSCs isolated from *in vitro*-fertilized embryos (embryonic stem cells) have a higher differentiation capacity than iPSCs but also possess ethical sensitivities and jurisdictional limitations (*100*). Other types of stem cells, such as synovial MSCs, also possess potential for development along the chondrogenesis pathway (*101*).

Adipose stem cells (ASCs) and the stromal vascular fraction (SVF)

In 2001, Zuk et al. (*102*) identified adipose tissue as a potential source of multipotent stem cells. Compared with BM-MSCs, ASCs can be obtained more easily and in larger quantities (*103*), have a longer lifespan (*104*), and possess immunosuppressive properties that mitigate inflammatory processes (*105, 106*).

In contrast to BM-MSCs, stem cells from fat can be separated relatively easily from lipoaspirate. The enclosed and automated ASC-isolation process Cytori (Lorem Cytori, San Diego, CA, USA) makes ASC introduction to operating theatres possible (*107, 108*). Single-staged intraarticular transplantation of Cytori-processed ASCs to treat OA has already been described by Garza et. al. (*109*).

Many clinical applications for ASCs have been identified, including demonstration of wound-healing properties in rodents (*110-112*), which was attributed to extracellular vesicle signaling that resulted in increased collagen deposition and vasculogenesis (*113*). Furthermore, decellularized adipose tissue-derived ECM hydrogel first described by Poon et al. (*114*) is potentially printable and supports ASC proliferation, as well as osteogenic differentiation of ASCs, to promote bone-defect repair *in vivo (115)*. Efforts towards cartilage restoration using ASCs have yielded new and clinically-translatable methods. O'Connell et al. (*116*) invented a "biopen" that enabled direct deposition of living cells and regenerative scaffolds during surgery.

A small fraction of the lipoaspirate (i.e., the SVF) contains a high concentration of ASCs (Figure 6), as well as preadipocytes and other precursor cells (e.g., pericytes and endothelial cells) that contribute to differentiation potential associated with cartilage regeneration (*117*). Compared with chondrocyte cocultures with ASCs, co-cultures with SVF may further enhance cartilage regeneration (*118*). A clinically-translatable approach described by Jurgens et al. (*119*), as well as a double-blind prospective study on knee OA, indicated greater clinical improvements observed following SVF injections as compared with standard hyaluronan injections (*120*).

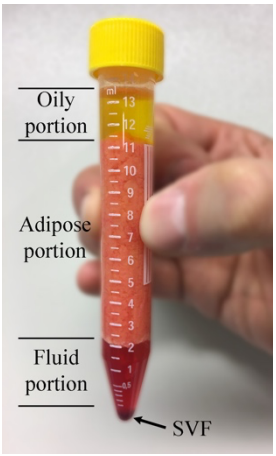

Figure 6. SVF. The lipoaspirate is stratified in distinctive layers. SVF can be extracted through various centrifugation, washing, and purification steps. This process can be partially automated. Another approach to extracting a stem cell-rich fraction is mechanical fractionation and lipoaspirate purification using the Lipogems system (Lipogems International SpA, Milano, Italy) (*121, 122*).

1.7 Biomaterials

The main function of biomaterials in 3D bioprinting technology is to mimic native ECM. Moreover, these materials must be printable, exhibit favorable rheological features (i.e., viscosity), have the capacity to be fixed post-printing, and possess long-term shape resilience. When introduced into a biological context, the biomaterial must also provide a favorable milieu for cells and be tolerated by the immune system. Many biomaterials have been assessed for 3D bioprinting applications, including natural and synthetic polymers.

Hydrogels are polymers that mainly comprise water (>98%). Natural hydrogels (e.g., cellulose and alginate) display many favorable biochemical properties, including biocompatibility and low cytotoxicity, making them suitable for utilization in 3D bioprinting. However, their innate viscosity properties limit the printing resolution.

Cellulose-based hydrogels

Hydrogels based on cellulose have been extensively evaluated for 3D bioprinting. Cellulose is a polysaccharide that originates from either a fermentation process of anaerobic bacteria (bacterial nanocellulose; BNC) or delamination of wood fibers. Recently, chemical decomposition of tunicates (i.e., tunicate nanocellulose; TNC) was also introduced as a novel source. After preparation, the smallest fractions of the resulting cellulose fibers (i.e., nanocellulose; NC) are separated and mixed with water to form a viscous gel.

Regardless of origin, NC possesses several favorable properties. The microstructure and porosity closely resemble native ECM and possess the ability to facilitate the transport of ECM proteins and signaling molecules (*123, 124*). Additionally, "smart" hydrogels have recently been developed, where the structural and mechanical properties of the biomaterials can be modified by changes in temperature and pH (*125-127*).

In addition to the use of NC as scaffolding material in 3D bioprinting, potential biomedical applications include wound repair (*128-132*) and burn-wound treatment (*133-135*). Although still at the preclinical level, NC-based 3D scaffolds reportedly enhance the proliferation of liver cell cultures (*136*).

Many studies show that NC is non-toxic and does not elicit an inflammatory response in a biological environment (*137-141*). Bacterial NC is already approved by the Food and Drug Administration (FDA) for human use, and TNC approvals are pending; however, NC is not biodegradable in humans because of a deficiency of degrading enzymes, which represents a limitation for some applications. Interestingly, in one study, the addition of cellulase to the cellulose-based hydrogel enabled subsequent breakdown of cellulose and added flexibility to cellulose-based biomaterials (*142*).

Alginate-containing hydrogels

Natural carbohydrates originating from seaweeds exhibit fast gelation and retain shape stability after 3D bioprinting and calcium cross-linking. However, high concentrations of alginate in bioink can easily clog the nozzle (*143*). A combination of NC and alginate (Figure 7), which is the bioink our group has mainly studied, provides synergistic properties, as the NC introduces an optimal microarchitecture, and the alginate provides filament-stabilizing cross-linking after printing, after which it dissipates.

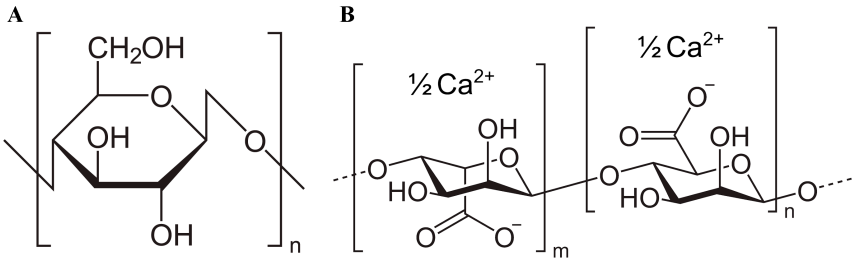

Figure 7. NC/alginate hydrogel. The components of the biomaterial used in our studies. NC (A) and calcium–alginate (B).

Synthetic hydrogels

PCL, the most widely used synthetic hydrogel, has a low melting temperature (60°C), cools rapidly after printing, and is both biocompatible and biodegradable, with an *in vivo* durability of up to 4 years (*144*), all properties that make PCL an attractive biomaterial for 3D bioprinting. Additionally, PCL is FDA-approved for use in humans. Several clinical applications have been investigated, including for neural regeneration (*145*) and bone-tissue engineering (*146-148*). One drawback in weight-bearing applications is that PCL is elastic and provides low mechanical strength; however, this weakness can be modified upon mixing PCL with other polymers, such as collagen (*149*). A combination of natural and synthetic hydrogels (e.g., NC/alginate and PCL) potentially offers the best options from two different worlds for cartilage-tissue engineering (*150, 151*).

NC origins

NC can be derived from plants, bacteria, and tunicates, each of which subsequently displays slightly different physical and chemical properties. However, they exhibit comparable biological and mechanical properties in several biomedical contexts and 3D bioprinting applications. Importantly, they are all non-toxic and biocompatible.

Plant-derived cellulose is the most abundant NC source and used in many industries. After pretreatment (pulping and bleaching), the diameter of the cellulose fibers is ~13 μm to 22 μm, with a crystallinity (i.e., structural order) ranging from ~44% to ~65% (*152*). Mechanical decomposition is required in order to obtain nanofibers. In addition to pure cellulose, NC also comprises hemicellulose, lignin, and pectin, which introduce complications in the purification

processes required to obtain plant-derived NC. Specifically, these purification procedures involve the production of toxic effluents that are harmful to the environment and potentially to biomedical applications (*153*).

Cellulose synthesized by bacteria forms at the nanoscale (diameter: ~10–100 nm; and crystallinity: 90%), can hold 99% water, resembles native collagen networks (*154*), and displays high mechanical strength and purity (*155*) along with high biocompatibility (*156*). Clinically interesting applications, such as auricular cartilage replacement (*157, 158*) and wound dressings with antimicrobial properties (*159, 160*), have been proposed; however, BNC comprises endotoxins, and large-scale production is challenging.

Novel TNC was used in studies **III** and **IV**, as well as an additional study from our group (*45*). TNC fibrils have similar dimensions as collagen and exhibit extremely high aspect ratios and crystallinity indexes (*161, 162*). Furthermore, TNC is ultra-pure and can be produced cost-efficiently in large quantities (*163, 164*). TNC contains very low endotoxin values while still benefitting from the physicochemical properties of BNC, making TNC highly suitable for biomedical applications in tissue engineering.

Biocompatibility

A basic requirement for a biomaterial intended for clinical use in humans is a high degree of biocompatibility. Ideally, the biomaterial should not cause acute inflammation, immunological rejection, or any long-term side effects. Because targeting and defusing foreign materials is the primary role of the immune system, evaluations of novel biomaterials for their biocompatibility represent an important step prior to clinical translation. For this purpose, a standardized process was developed by the international organization for standardization (ISO). ISO protocol 10993-6 annex E is specifically applied to address biomaterial evaluations and allows comparison of in-depth evaluations with those of other well-known biocompatible materials. In study **IV**, we used the clinically relevant and inert control biomaterial expanded polytetrafluoroethylene (ePTFE; i.e., Gore-Tex) to establish a comparable result. Briefly, *in vivo* evaluation was performed using histopathologic analyses targeting inflammatory cells (e.g., polymorphonuclear cells, lymphocytes, and

macrophages), fat infiltration, fibrosis, necrosis, and neovascularization, resulting in a comparable biocompatibility score.

1.8 3D Bioprinting

There are three major modalities: extrusion, stereolithography, and inkjet-based bioprinting (Figure 8). Each method has its advantages and limitations; however, they all demonstrate a rapid technical evolution and the fact that the technologies have become progressively cheaper and, thus, more widespread. Additionally, a fourth modality, integrated tissue organ printer, has recently emerged (*165*), with this technique using pneumatic microextrusion and combining a cell-laden hydrogel with synthetic polymers to enable more complex applications, such as human-sized organ bioprinting. Computer-aided design technologies feed bioprinters with patient-specific data, thereby enabling the production of anatomically accurate, 3D-bioprinted results.

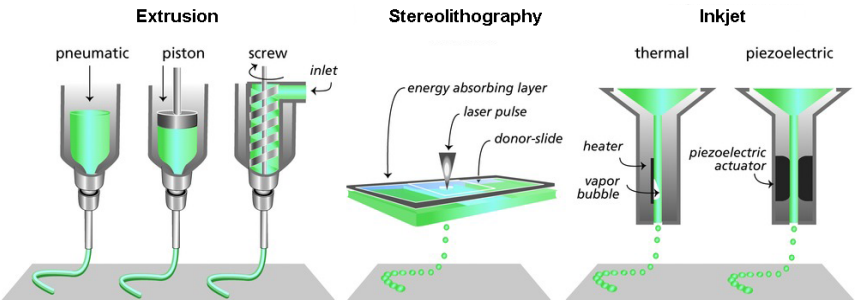

Figure 8. Bioprinting modalities. Schematic overview of the extrusion (*left*), stereolithographic (*middle*), and inkjet (*right*) methods. Adapted from Malda et al. (*166*) and reproduced with permission.

Extrusion bioprinting

The biomaterial–cell mix is dispensed through a nozzle using pneumatic or mechanical pressure. Multiple layers are then added to the 2D pattern in order to create a 3D construct. Additionally, several printing heads containing different cell types can be used simultaneously to create composite constructs that contain high densities of homogeneously distributed cells (*167*). Moreover, spheroids and high-viscosity fluids, such as polymers, can be used, as well as low-viscosity hydrogels, depending on the desired biological and

mechanical properties. Drawbacks include relatively low resolution (~100–200 microns) (*168, 169*), and that living cells are sensitive to pressure, turbulence, and shear stress induced by the nozzle (*170*). A novel extrusion method (i.e., cell electrowiring) was recently developed to achieve higher resolution (*171*).

Stereolithography bioprinting
This method uses light at different wavelengths to structurally arrange a photopolymerizable bioink with very high precision, resolution, and speed. However, because of the few variants of ideally biocompatible photopolymers, bioprinting of living cells is limited (*172*).

Inkjet bioprinting
Inkjet bioprinting (also termed droplet-based bioprinting) actuated by temperature or voltage can distribute cells in certain areas of the construct with high precision in a highly controllable setup. Moreover, this technique allows for the use of different cells and biomaterials heterogeneously distributed within a construct (*167*). One drawback is that this technique can only use low-viscosity (i.e., liquid) bioinks.

1.9 Introduction to the assessments of 3D-bioprinted cartilage-like implants in studies I through IV

Animal models
Two animal models were used for studies **I** through **IV**: nude mice and Wistar rats. Specifically, these included female mice (*Mus musculus*) from the nude BALB/c substrain. Importantly, this animal model lacks a thymus and is, therefore, unable to produce T cells. This immunodeficiency enables the transplantation of cells and tissues from other species without significant rejection; however, the mice have the capability to mobilize a humoral immune response involving B-cell production.

The Wistar rats used in study **IV** is an outbred albino rat with a competent immune system, which meant that only autologous cells could be transplanted. Importantly, if human cells were mixed in the bioink, these rats would require immunomodulatory treatment;

however, in study **IV**, our focus was assessment of the biocompatibility of the TNC biomaterial, and no cells were mixed into the bioink.

Histomorphology

We used Alcian Blue van Gieson staining to evaluate cartilaginous tissue architecture. The basic Alcian Blue stain binds to acidic GAGs, whereas the van Gieson component (a mixture of picric and fuchsin acids) stains collagen. Additionally, we used Safranin-O to verify the acidic proteoglycan content. Furthermore, we used hematoxylin and eosin staining to better detect the overall microscopic anatomy, as well as vascular content. Hematoxylin is a basic stain, and eosin is acidic and stains basic structures. In study **III**, we used von Kossa staining (i.e., silver nitrate) to visualize calcium deposits as an indication of potential mineralization. These different staining protocols allowed assessment of the ECM and manual counting of chondrocyte nuclei and clusters, as well as detection of plausible adverse reactions, such as ossification, inflammation, necrosis, and/or tumor formation.

Immunohistochemistry

Complementing the histomorphologic evaluation, we performed immunohistochemical analyses to further characterize the microenvironment inside the 3D-bioprinted constructs. Type II collagen is expected to be present in the territorial matrix that surrounds thriving, proliferating chondrocytes. ColX is typically expected in hypertrophic cartilage, and morphological signs of hypertrophic chondrocytes and the presence of ColX suggest that the cartilaginous tissue has entered the endochondral pathway towards bone formation. Ki-67, a protein present during all active phases in the cell cycle and mitosis, is typically used as an indicator of cell proliferation.

Fluorescence in situ hybridization (FISH)

To confirm that the chondrocytes originated from male donors and were not differentiated from the female stem cell donors, we performed FISH analyses. Briefly, the FISH probe binds to the centromere region of chromosome X and satellite III DNA at the Yq12 region of chromosome Y, enabling visualization of the results via

fluorescent probes (chromosome X in green, and chromosome Y in red).

Magnetic resonance imaging (MRI)
MRI takes advantage of the spinning polarization of hydrogen atoms in water molecules. Using radiowave pulses to excite the spin energy transition, the magnetic field can locate the change in polarization, resulting in a map over different areas within an organ or any tissue depending on its water content.

MRI can longitudinally evaluate tissue perfusion and diffusion dynamics *in vivo* and is currently widely used in clinics to assess functional aspects of brain circulation, tumor characteristics for diagnostics and treatment effects, coronary heart artery-perfusion details, and providing critical details of a damaged meniscus preceding orthopedic surgery.

MRI technology can also be used to detect and monitor evolving vessels inside of 3D-bioprinted constructs over time using intravenous contrast agents. Although native cartilaginous tissue lacks blood vessels, the proximity to oxygen and nutrient-transporting circulation and diffusion is crucial for cartilage survival. Moreover, in composite organs, other areas may need direct access to the blood circulation.

2. Aims

The aims of this thesis are:

1. To assess the proliferative potential of 3D-bioprinted chondrocytes.
2. To evaluate the long-term stability of 3D-bioprinted cartilage-like constructs and their potential adverse effects (e.g., necrosis, ossification, and tumor formation) induced by the implantation.
3. To analyze the vascularization process inside gridded 3D-bioprinted cartilage-like constructs.
4. To evaluate the biocompatibility and biomechanical properties of the novel TNC bioink.

3. Methods

3.1 3D bioprinting

The 3D bioprinter
Throughout the studies, we used extrusion bioprinters (INKREADIBLE, INKREADIBLE+, and BioX; Cellink AB, Gothenburg, Sweden) (Figure 9). These printers have multiple interchangeable printheads and a resolution of 100 µm to 200 µm. To preserve cell viability, we used the lowest possible extrusion pressure while retaining sufficient resolution, and conical nozzles were used to minimize turbulence.

Figure 9. Extrusion bioprinting. The BioX extrusion bioprinter offers excellent parameter control and reproducibility. The three printer heads allow for composite depositions. Image from the product manual (Cellink AB).

The bioink scaffold
In studies **I** and **II**, we used BNC-based bioink, and in studies **III**, and **IV**, TNC-based bioink was used. The NC bioinks were supplemented with alginate for calcium-induced cross-linking post-

printing at a mixing ratio of 80:20 (BNC or TNC to alginate). The dimensions of the constructs used for the nude mouse model were 5 × 5 × 1.2 mm (**I**), 6 × 6 × 1.2 mm (**II**), and 10 × 10 × 3 mm (**III**), with a grid spacing of 0.6 mm. The Wistar rats in study **IV** carried four constructs with a dimension of 10 × 10 × 1 mm.

3.2 Cells

Chondrocytes were obtained from redundant cartilage during septoplasties, and the MSCs were obtained from Rooster Bio (Frederick, MD, USA). The SVF was enzymatically (collagenase) and mechanically separated from redundant adipose tissue after cosmetic liposuction procedures.

Total cell number and viability were determined using the Trypan Blue exclusion method, and Cell Counter (Thermo Fisher Scientific, Waltham, MA, USA). All experiments were conducted using human nasal chondrocytes (hNCs) and MSCs at passage two.

In studies **I** and **II**, the cells and biomaterial were mixed at a 1:11 ratio. In study **III**, the cell to biomaterial ratio was 1:10. In all studies, the cell density of the implants was 10×10^6 cells/mL bioink.

3.3 Animal experiments

The nude mice in studies **I** through **III** were 8-weeks old and weighed ~20 grams at the start of the experiments. The animals were anesthetized using intraperitoneal injection of ketamine (50 mg/mL) and medetomidine (1 mg/mL) at a 1.5:1 ratio (**I** and **II**) or with gas (isoflurane) (**III**).

The Wistar rat model in study **IV** weighed ~200 g at day 0 and was anesthetized with 2% to 3% isoflurane.

The animal experiments in studies **I**, **III**, and **IV** lasted from 60 to 100 days, whereas the long-term study **II** lasted 10 months.

3.4 Post-explantation assessment

Mechanical properties
Mechanical analyses of the constructs in study **II** were conducted after printing and cross-linking using a universal testing machine

(model 5565A; Instron, Norwood, MA, USA) and compared with measurements after explantation (after 8 and 10 months). The cylindrical indenter measured the degree of biomaterial deformation relative to the pressure applied and correlated to the construct areas. The unconfined compression and stiffness (i.e., Young's modulus) were tabulated and graphed as a function of time.

Histomorphology

Our standard staining protocol with Alcian Blue van Gieson (ABvG) was used in all experiments. Additionally, Safranin-O, hematoxylin and eosin, and von Kossa staining protocols were applied. The sections were analyzed using light microscopy.

Immunohistochemistry

To visualize type II collagen production (in studies **I** and **III**), we used a monoclonal mouse IgG antibody (1:300; clone II-4C11, cat. No. 63171; MP Biomedicals, Irvine, CA, USA) conjugated with a fluorescent goat anti-mouse IgG (1:300; AlexaFluor 546, A11030; Invitrogen, Carlsbad, CA, USA).

Endothelial cells lining vascular structures in study **III** were detected with a human anti-CD31 antibody (1:200; clone EP3095, ab134168; Abcam, Cambridge, UK).

The proliferation rate in study **II** was assessed with Ki-67 using a monoclonal mouse anti-Ki67 IgM antibody (1:400; ab6526, clone PP-67; Abcam).

ColX in study **III** was analyzed using a monoclonal mouse anti-ColX IgM antibody (1:200; ab49945, clone COL-10; Abcam) and monoclonal rabbit anti-ColX IgG antibody (1:200; ab182563, clone EPR13044; Abcam).

FISH

In study **I**, we used a Vysis CEP X/Y probe (cat. No. 07J22-050; Abbot Laboratories, Chicago, IL, USA) to detect the chondrocyte phenotype. Nuclei were counterstained with 4,6-diamidino-2- phenylindole.

MRI

In study **III**, a tail catheter was applied to administer a gadolinium-based contrast agent (0.1 M Gd-DTPA; Dotarem; Gothia Medical Billdal, Sweden) at 0.3 mmol/kg body weight. We used a 7 T MR

system (BioSpin 70/20AS AVANCE 1 using ParaVision 5.1; Bruker Daltonik, Bremen, Germany), and each MRI session lasted ~75 min per mouse. The mice were scanned sequentially at days 0, 7, 30, and 100. MRI data were post-processed, and the diffusion and perfusion parameters were calculated for each voxel for compilation as functional color maps.

Statistical methods

An independent Student's *t* test was used to compare the mean number of cells between groups in study **I**. Histograms were used to ascertain normal data distributions in study **III**, enabling comparisons between medians and interquartile ranges. The non-parametric data in studies **II** and **IV** were analyzed using a Mann–Whitney *U* test to detect differences between two unrelated groups.

3.5 Study design

Study I
3D-bioprinted constructs containing a scaffolding material (i.e., bio-ink) mixed with stem cells and chondrocytes were subcutaneously implanted in 48 nude mice divided into four groups for 30- and 60-day evaluation, respectively. The constructs were evaluated morphologically, immunohistochemically, and using FISH. For morphological analysis, GAGs in the ECM of chondrocytes were visualized with ABvG, and all nuclei-bearing cells stained with ABvG (i.e., chondrocytes) were counted manually.

Study II
A total of 16 3D-bioprinted cell-laden constructs were implanted subcutaneously in 16 nude mice. Eight constructs had 20% hNC and 80% hBM-MSCs, and the other eight comprised 20% hNC and 80% SVF. Four animals in each of these two groups were studied for 8 months, and the other four for 10 months. In parallel, a control group of six mice carried cell-free constructs.

Study III
The vascularization process of subcutaneously-implanted 3D-bioprinted gridded constructs was sequentially assessed on days 0, 7, 30, and 100 using MRI. Ten animals carried chondrocyte-containing constructs, and another 10 carried cell-free constructs. Following explantation, all constructs underwent histologic and immunohistochemical analyses.

Study IV
TNC discs were subcutaneously implanted into 24 Wistar rats (n = 4 discs/animal) for study periods of 30 and 90 days. We used ePTFE (Gore-Tex) as a control. Histopathologic evaluation of each disc and the surrounding tissues was performed according to the ISO standard.

Table 1. Detailed overview of the study methods (**I–IV**).

		Study I	Study II	Study III	Study IV
Published		dec 2017	jun 2020	jun 2021	submitted
Study time (months)		2	10	3	3
Biomaterial/Alginate (ratio, vol%)		BNC:Alg (80:20)	BNC:Alg (80:20)	TNC:Alg (80:20)	TNC:Alg (80:20)
Bioprinter	Printer model	INKREADIBLE	INKREADIBLE	INKREADIBLE +	BioX
	Printing pressure (kPa)	12–20	10–19	11–13	16–17
Constructs	Dimensions (mm)	5 × 5 × 1.2	6 × 6 × 1.2	10 × 10 × 3	10 × 10 × 1.2
	Crosslinking ($CaCl_2$)	$CaCl_2$	$CaCl_2$	$CaCl_2$	$CaCl_2$ and $BaCl_2$
Cells	Cell types	hNC/ MSC	hNC/ MSC or SVF	hNC	No cells in vivo
	Cell density/ml bioink	10×10^6	10×10^6	10×10^6	-
	Viability (%)	-	≥ 96	≥ 98	-
	Cell ratio	20 hNC:80 MSC	20 hNC:80 MSC/SVF	-	-
	Cells vs Biomaterial	1:11	1:11	1:10	-
Animals	Species	BALB/C	BALB/C	BALB/C	Wistar rats
	Number of animals	48	25	20	24
	Number of implants	48	25	20	96
	Age (weeks) day 0	8	8	8	-
	Weight (g) day 0	20	20	20	150–200
	Anesthesia	Inj. (Ketamine/ Medetomidine)	Inj. (Ketamine/ Medetomidine)	Gas (Isoflurane)	Gas (Isoflurane)
Analyses	IHC	Collagen-II, Ki67	-	CD31, Collagen-II, Collagen-X	-
	Histology	ABvG, Saf O	ABvG, Saf O	ABvG, Htx-eosin, Saf O, von Kossa	Htx-eosin, von Kossa
	FISH	x	-	-	-
	MRI	-	-	x	-
	Biomechanical	-	Instron	-	

3.6 Ethics

All animal experiments were conducted according to institutional, national, and European guidelines and regulations at the core facility for experimental biomedicine at the University of Gothenburg, Sweden, and approved by the Ethics Committee for animal experiments at Sahlgrenska University Hospital. All human cells and tissues were donated after informed consent and approved for use by the appropriate ethical authority. Some of the cell harvestings were performed by our partners in Germany, and these procedures were approved by the appropriate ethical committee in Berlin, Germany.

Ethical approvals:

1. Dnr 119–2015; Ethics Committee for Animal Experiments at Sahlgrenska University Hospital/Gothenburg University, Göteborg, Sweden.
   The initial approval concerning the implantation of 3D bioprinted constructs subcutaneously in nude mice.

2. Dnr 36–2016; Ethics Committee for Animal Experiments at Sahlgrenska University Hospital/Gothenburg University, Göteborg, Sweden.
   Additional approval for the MRI experiments on nude mice.

3. Dnr 624–16; Ethics Committee for Animal Experiments at Sahlgrenska University Hospital/Gothenburg University, Göteborg, Sweden.
   Approval for the usage of redundant human tissues.

4. Dnr 5.8.18-09289/2020; Ethics Committee for Animal Experiments at Sahlgrenska University Hospital/Gothenburg University, Göteborg, Sweden.
   Renewal of the ethical approval (Dnr 119–2015) concerning the implantation of 3D bioprinted constructs subcutaneously in nude mice.

5. Dnr 5.8.18-04945/2020; Ethics Committee for Animal Experiments at Sahlgrenska University Hospital/Gothenburg University, Göteborg, Sweden.
   Approval for implantation of 3D bioprinted constructs simultaneously in Wistar rats.

Additional ethical approvals:

6. EA1/169_12; Ethics Committee at Charité Universitätsmedizin in Berlin.
   Approval for the usage of redundant cartilaginous tissue from rhinoplasty procedures.

7. Dnr S040–01; Ethics Committee at Sahlgrenska University Hospital/Gothenburg University, Göteborg, Sweden.
   Approval for the positive controls used in the immunohistochemical analyses.

4. Results

4.1 Study I

Forty-eight mice were included, and 41 completed the study period. The expected type II collagen production in the ECM was visualized immunohistochemically and corroborated the ABvG staining. The number of chondrocytes and cluster formations increased significantly between days 30 and 60. Addition of stem cells significantly enhanced chondrocyte proliferation. FISH analysis confirmed that the chondrocytes had a male phenotype, which verified the male chondrocyte-donor origin.

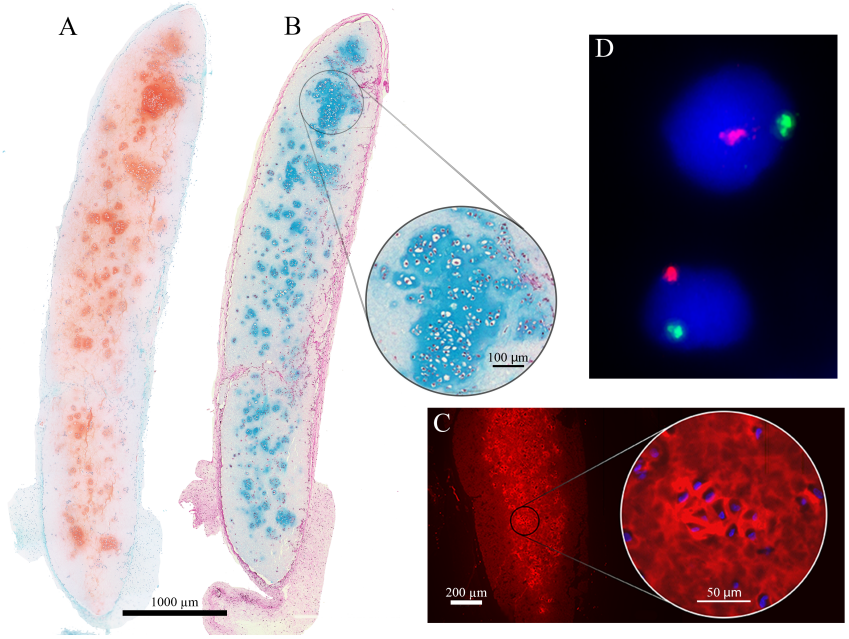

Figure 10. Human chondrocytes in the NC-based biomaterial. Histological sections stained with Safranin-O (A) and ABvG (B). Red clouds (A) indicate positivity for proteoglycans, and blue clouds (B) indicate GAGs in the ECM. Magnification in (B) shows a large chondrocyte cluster comprising >50 chondrocytes with black nuclei and confluent GAG-positivity in the territorial matrix. Immunohistochemical analyses (C) corroborated the

histological findings, with collagen type 2 positivity observed in the GAG- and proteoglycan-positive areas. FISH analysis (D) indicated that the proliferating chondrocytes exhibited a male phenotype, as visualized using fluorescent probes (green: X-chromosome; red: Y-chromosome). Bars: 1000 μm (A, B), 100 μm (B magnification), 200 μm (C), and 50 μm in (C). The images were cropped and adjusted for contrast and exposure.

4.2 Study II

In total, 20 of the 22 mice completed the entire study period. We observed no signs of necrosis, tumors, bone formation, or other adverse effects. The constructs were well-preserved, and histologic analyses showed thriving, proliferating chondrocytes in cartilage-like formations, with no significant difference observed between the hNC/BM-MSC and hNC/SVF groups. The cell-laden constructs exhibited significantly improved unconfined compression strength and compressive modulus over time relative to the cell-free controls.

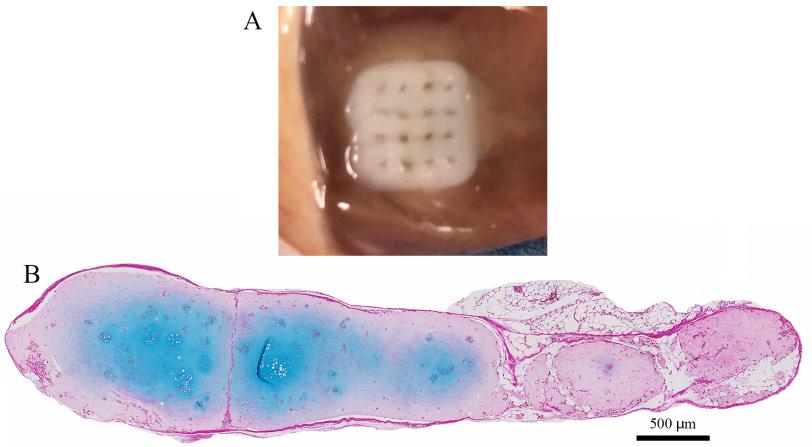

Figure 11. Long-term resilience of 3D-bioprinted cartilage-like constructs. Macroscopic image of the gridded implant *in situ* after 10 months *in vivo* (A). A cross-sectional display of one hNC construct shows an abundance of thriving chondrocyte clusters. The cross-sectional histologic segment was stained with ABvG, which highlighted the GAGs in blue (B). Bar: 500 μm. The image was cropped and adjusted for contrast and exposure.

4.3 Study III

In total, 18 of the 20 mice completed the entire study period and showed cartilage-like tissue established inside the constructs. Hot spots in the grid holes of the cell-containing constructs according to perfusion MRI confirmed functional circulation established via

ingrowth of blood vessels from the host. Diffusion MRI demonstrated a high diffusion coefficient of the TNC biomaterial (2.6 $\mu m^2/ms$) and its sustained stability over the entire 3-month study period. Histologically, we observed cartilage-like formations and proliferating chondrocytes, and immunohistochemical analyses confirmed that the vascular structures were lined with endothelial cells. There were no signs of ossification or necrosis.

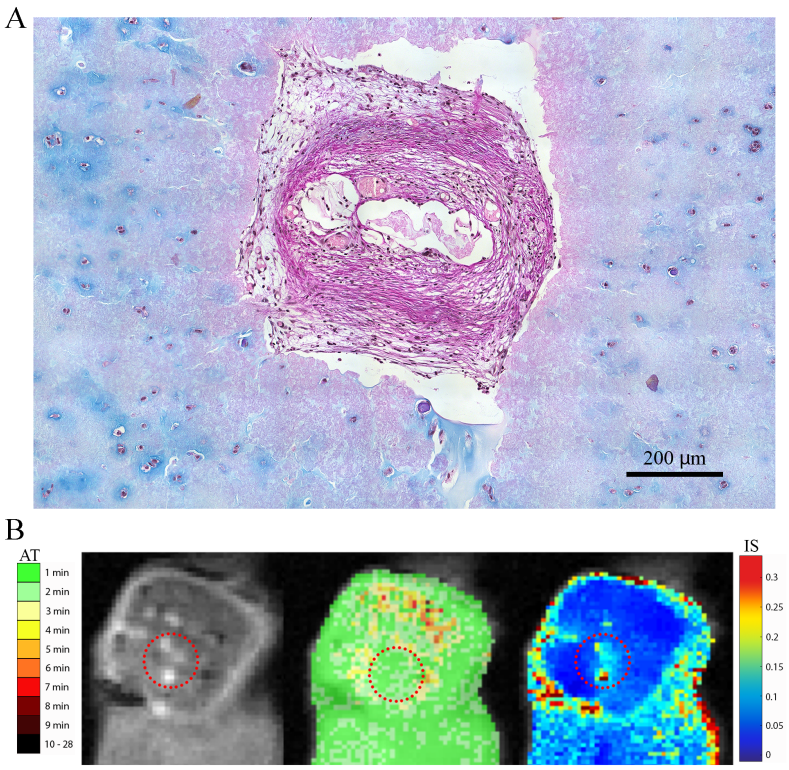

Figure 12. Blood vessel development inside a 3D-bioprinted construct. Histological section stained with ABvG after 100 days *in vivo* (A), with the area of focus showing one of the grid holes filled with connective tissue, vessel structures, and erythrocytes. The near surroundings of the grid hole comprise mainly biomaterial, and further away, chondrocytes reside at a distance, where the oxygen pressure is ideal. Bar: 200 µm. The chondrocyte-containing constructs displayed contrast hot spots (*red circles*) in the grid holes according to MRI at day 30 (B, *left*). The superimposed color maps indicate that the contrast arrived early [i.e., short arrival time (AT)] (B, *middle*) and with a steep initial slope (IS; i.e., high IS) (B, *right*) as compared with the cell-free controls. Appraisals of AT and IS in the aorta indicated that the blood vessels in the constructs were interconnected with the systemic circulation. The images were cropped and adjusted for contrast and exposure.

4.4 Study IV

All 24 Wistar rats thrived throughout the study period, and the TNC biomaterial showed excellent rheologic and printability properties. The biocompatibility was within the same range as ePTFE according to ISO 10993-6, and there were no signs of necrosis or any other adverse events. We concluded that TNC is highly suitable for bioprinting and clinical applications. This study has been submitted for publication.

5. Discussion

3D bioprinting is on the verge of a focus shift from laboratory *in vitro* studies and rodent experiments to clinical trials on more complex species and humans. Within a few years, this tissue-engineering technique will be further fine-tuned, and many of the associated biological concerns will likely be resolved to a degree that permits proceedings to human trials. This doctoral thesis presents some basic scientific knowledge promoting this translational process.

There previously existed a lack of knowledge regarding quantitative aspects of chondrocyte proliferation in 3D-bioprinted constructs, which made comparisons and validation between studies difficult. In studies **I** and **II**, we focused mainly on biomaterial characterization in relation to human cells, as well as basic biological concepts, such as proliferation and matrix production, associated with cartilage formation. As suggested by other studies (*173-177*), we were able to quantitatively confirm that the presence of stem cells boosted chondrocyte proliferation. Furthermore, we showed that an NC and alginate mixture is a biomechanically viable biomaterial for use in 3D bioprinting technology.

Another critical challenge is the longevity and safety of a 3D-bioprinted feature that has been transplanted to a patient. In addition to long-term loss of material-specific properties, material fatigue, and dissolving, any foreign material can potentially cause adverse effects. A clinical example is silicone breast implants, which can cause breast implant-associated anaplastic large cell lymphoma, although this is rare (*178*). Another clinically relevant breast implant-related problem is fibrosis, where the foreign-body reaction eventually encapsulates the implant, creating discomfort in some patients and in some cases even necessitating explantation. To evaluate such long-term adverse events that are intimately connected to human immunology, rodent animal models are insufficient.

Although we have not evaluated our methodology in higher or more complex species than rodents, some extrapolations and

predictions are possible from the results of studies **I** and **II**. These include assessment of the basic biological behavior of human chondrocytes (proliferation, clustering, and cartilage formation). Furthermore, the 3D-bioprinted scaffolds withstood the long-term biological pressure imposed by the *in vivo* model.

In our first studies, we successfully used commercially available stem cells (hBM-MSCs) mixed with human chondrocytes obtained from biopsies from the nasal septum. In the following studies, the acquisition of autologous stem cells evolved to clinically more relevant methods using adipocyte stem cells and SVF.

One major challenge of 3D bioprinting technology and confronted by the global scientific community is the upscaling of 3D-bioprinted constructs to human-sized proportions. The main obstacle is the need for vascularization; the more voluminous the tissues, the greater the oxygenation and nutritional demands. To support other adjacent tissues dependent on direct perfusion and connection to host circulation, the cartilage-like constructs need to be able to carry blood vessels. For example, an overlying fasciocutaneous flap is dependent on direct oxygenation and nutrient transfer. Alternatively, these must be supplied via a complex microsurgical anastomosis. Additionally, for composite constructs containing different kinds of cells, the needs for perfusion and oxygenation vary. Study **III** aimed to map out the details of vascularization of gridded 3D-bioprinted cartilage-like constructs with the goal of counteracting anoxic cell death and facilitating vascularization. We primarily applied three concepts in study **III**.

First, we showed that the TNC/alginate biomaterial (used in studies **III** and **IV**) displayed excellent and sustained diffusion properties that were comparable to that of free water (diffusion coefficient: TNC/Alginate, 2.6 $\mu m^2/ms$ vs. free water, 3.0 $\mu m^2/ms$). Thus, the biomaterial ensured an excellent delivery capacity to central parts of the constructs. A long-term high and stable diffusion coefficient was an important observation that likely explained why the cells in the middle of the constructs survived despite their residing in an area beyond the theoretical maximum diffusion distance. These findings confirmed that the diffusion properties of the biomaterial are crucial to supporting the cells until neovascularization is established.

Second, we used gridded constructs, where the pores provide close access to all parts of the bioprinted tissue. This physical architecture decreases the diffusion distance between the chondrocytes inside the constructs and the host environment. Additionally, regarding composite constructs comprising chondrocytes and additional cell types, the grid holes promote neovascularization.

Third, we evaluated the diffusion and evolving perfusion properties using an already clinically integrated modality in order to assess vascularization inside the cartilage-like constructs. Therefore, the evaluation and monitoring of transplanted constructs can be more easily implemented and standardized in clinical studies.

The concept of gridded scaffolds originated from the difficulties of oxygenating central parts of a solid tissue construct. Moreover, gridded scaffolds display a larger area-to-volume relationship than a solid construct. Consequently, central areas of the construct are available to the surrounding ECM and expose residential cells to the microenvironment, thereby enabling an exchange of oxygen and nutrients. Theoretically, the diffusion limit is ~200 µm; thus, the largest possible construct size would be 400 µm (*165*). However, we have printed constructs 3-fold larger without any viability issues. This is likely due to several supporting factors. Chondrocytes are sturdy and resilient cells that natively thrive in a low-oxygenated environment, which allows them to withstand transient oxygen depletion to a larger extent than other cell types. For example, adipose cells have higher demands for oxygen, although we showed that adipose tissue also survives inside of constructs with a size exceeding the diffusion limit (*46*). Supposedly, this can be attributed to the excellent diffusion properties offered by the used biomaterials (*45*), as well as rapid vascularization. Furthermore, even if the best possible biomaterial (i.e., with a diffusion capacity close to that of water) is used, the diffusion distance in scaffolds with larger dimensions remains a limiting factor.

Theoretically, a combination of adipose and cartilaginous tissues arranged in layers in a gridded scaffold would offer several advantages. The adipose tissue brings stem cells that boost chondrogenesis and provide building blocks for vasculogenesis. In addition to study **III**, we also demonstrated an interconnection between human vascular components and systemic circulation in the rodent host

(*45*). Specifically, we observed coupling of native vessel structures included in the lipoaspirate with host vessels that infiltrated via the grid holes.

Furthermore, in study **IV**, we observed an abundance of vessels and adipose tissue infiltrating the constructs, indicating that the fundamental properties allowing for vasculogenesis were met by the TNC biomaterial.

Other approaches to vascularize 3D-bioprinted constructs include direct printing of channels, self-folding tubes, and sacrificial inks.

In a not-yet-published study, we used protein-coated bioink surfaces to promote the vascularization of 3D-bioprinted constructs. Preliminary results indicated that the bioconjugated ECM proteins laminin, fibronectin, and collagen type I provided human endothelial cells enhanced cell-adhesion possibilities and higher viability. Another variant of direct printing was described by Jia et al. (*179*), who used a three-component bioink to create tubular structures inside the scaffold.

Self-folding tubes are biomaterials with the ability to fold into tubular structures post-printing and accomplished via cross-linking gradients. However, this method is currently limited to tubes at the micro-scale, although this has recently been further developed to the millimeter-scale (*180*).

Previous studies described the testing of composite scaffolds encompassing a sacrificial biomaterial component (e.g., gelatin) (*181, 182*). Briefly, the sacrificial bioink is printed in strings inside the construct, after which it dissipates post-printing and leaves a tubular void. Notably, the surrounding biomaterial remains stable. Subsequently, these channels can be infiltrated by host vessels.

Originality and clinical relevance

We published our novel method for creating human cartilage-like tissue in 3D-bioprinted constructs in a pilot study in 2017 (*183*) and performed an in-depth evaluation of the methodology later that year in a larger study (**I**). The clinical relevance involved the use of human cells in an animal model. Because there was a lack of longitudinal, long-term data for 3D-bioprinted cartilage-like constructs, we also conducted a 10-month study addressing long-term issues (**II**).

Later, in collaboration with a radiation physicist, we introduced a novel method for evaluating vascularization inside of the constructs using MRI (**III**). This approach had not previously been employed in this context, and because MRI is a clinically well-established modality, this brought the 3D bioprinting methodology closer to clinical translation. Because our model relies on spontaneous ingrowth of blood vessels, we performed no chemical manipulation to induce or stimulate vascularization. In parallel with MRI evaluation of the cartilage-like constructs, we also assessed adipose tissue (*45*). In both MRI studies, we used the novel TNC bioink and subsequently evaluated its mechanical properties and biocompatibility in study **IV** using an immunocompetent animal model along with a control group carrying Gore-Tex implants (a well-known biocompatible material extensively used worldwide on humans).

Representativeness

The representativeness of the nude mouse model used in the studies outlined in this thesis must be valued mainly as a biochamber and not as a substitute for human trials. In this regard, the results are transferrable between species; however, the model does not allow an assessment of the overall immunological interactions that occur in a human host. For example, the behavior of human chondrocytes can be studied in a biological context, even though they are unaffected by any graft-versus-host reactions. However, cartilaginous tissue is highly dependent on its surroundings and, therefore, inadequate surroundings lacking critical immune system components (e.g., T cells) cannot be extrapolated beyond the laboratory setting. However, BALB/C nude mice harbor an intact humoral immune system, allowing them to initiate a B-cell-mediated response to the implants, suggesting intact complement activation, including inflammation and phagocytosis.

The standard experimental setup involved one or more study groups and one parallel control group. The size of each study group was generally six animals in order to allow detection of statistically significant differences. This group size was determined from the results of our pilot study (*183*). A post hoc power analysis was also performed after study **I**, resulting in >99% power when using groups of six and a low risk for type II errors.

Throughout the studies, we have used a significance level of 95% (i.e., $p < 0.05$; the risk for type I errors was 5%). The methods were meticulously chosen according to the initial hypotheses and balanced by the practical possibilities, as well as conscious restrictions to keep the number of animals used as low as possible.

Validity

The validity of the studies outlined in this thesis was ensured by the use of standardized and previously well-established methods adapted to the intent and context of the hypotheses. For example, cartilaginous tissue comprising healthy, proliferating chondrocytes produce GAGs, proteoglycans, and type II collagen. Therefore, the analyses focused on the detection of these compounds using standard analytical methods.

MRI has been extensively used clinically for decades to detect physiological changes in soft tissue and tumors (*184*). This method allows the longitudinal and objective measurement of neovascularization and biomaterial properties in detail using perfusion and diffusion parameters.

Reliability

The reliability of our results was demonstrated in the accuracy of the cell count reported in study **I**. To minimize subjective errors in these kinds of assessments, we used repeated counting, as well as different evaluators, and accounted for interindividual variance. Other examples of reliability include the qualitative evaluations related to immunohistochemical and histologic analyses. All results were carefully interpreted and discussed within the research group, as well as by external experts. For example, in study **IV**, histomorphology assessments were performed by an external pathologist in addition to the two evaluators from within the research group. Finally, the publications have been reviewed and scrutinized through impartial peer review.

Limitations

Logistical, ethical, and biological limitations must be addressed and considered when designing studies and interpreting the results from animal studies. The number of animals used must be large enough to provide a statistical certainty of potential differences. On the other hand, we are ethically obliged to reduce the experimental cohorts to

a minimum. When planning the studies, we aimed at groups of six in order to gain statistical power and allow us to either prove or discard our hypotheses.

The physical dimensions of the nude mice only allowed implantation of one construct, whereas the larger Wistar rats could easily carry four constructs subcutaneously on their backs. Therefore, the rats could serve as their own controls, which allowed the number of animals needed to be reduced.

The longevity of nude mice ranges from 6 to 18 months (*185-187*), and the lifetime of the BALB/C sub-strain used in our studies is estimated at 12 months. Extrapolations of biological scenarios over long periods are challenging. Specifically, in the nude mouse model, diseases and physiological decline related to senescence are likely to appear after ~6 months. Furthermore, BALB/C mice are inclined to develop lymphoreticular neoplasms (*186*). Although unrelated to the chondrocyte lineage, such predispositions distract other biological implications.

Study **I** was limited by the use of only two cell donors. One donor provided the hBM-MSCs, which introduces the uncertainty of inter-individual differences (e.g., proliferative capacity). Siegel et al. (*188*) showed that donor characteristics affect hBM-MSC functional properties. Additionally, both the harvesting and target location can affect chondrocyte functionality (*189*) and immunogenicity (*190*). Another limitation concerns the study design. In study **I**, we replaced 80% of the chondrocytes with stem cells. Another option could have been the addition of stem cells to the mixture while maintaining the same total number of chondrocytes in all groups. Theoretically, that would have been a more commensurable setup.

Study **II** includes four noteworthy limitations. First, the nude mouse model is not ideal for evaluating our hypotheses, given that the results cannot easily be translated to a human context due to the lack of T cells. Second, the longevity of this animal model (i.e., ~12 months) and its innate tumor susceptibility poses challenges when attempting to translate the results to human physiology. Third, the number of animals in each group was small, resulting in potential difficulties in detecting differences. Fourth, to strengthen our conclusions, we should have included a fourth group comprising only chondrocytes without stem cells.

In study **III**, we claimed that the cell-containing constructs were vascularized through the grid holes and identified as contrast hot spots, whereas no hot spots were observed in the cell-free controls. However, confirmation of these findings requires an additional study conducted using larger groups and an increased number of MRI checkpoints, as well as the addition of a group comprising solid constructs for comparison. Additionally, in study **III**, we used only six cell-free control constructs that met two or three of the MRI checkpoints. It should be noted that vascular structures were also identified in the cell-free constructs, and it is possible that the hot-spot phenomena also appeared in these controls between days 30 and 100 but remained undetected. Furthermore, MRI measurements are highly dependent on the chosen region of interest. Although we used the mean of many frames, subjective errors inevitably occurred.

In study **IV**, we could have used immunohistochemistry to further strengthen our assertions, even though this is not required by the ISO protocol. For example, although histology was evaluated by an expert pathologist specialized in inflammation, further details would have been revealed with higher accuracy by immunohistochemical analysis. Additionally, the standardized ISO protocol is vague regarding the details involved in complex inflammatory processes. Therefore, we elaborated these details in the manuscript, which introduced further subjectivity and makes comparisons to other studies challenging.

The experience derived from struggles and failures

The scientific journey during the research associated with this dissertation has offered me a tremendous amount of knowledge and pleasure, as well as a fair amount of frustration. Between 2015 and 2021, our research group conducted >25 animal trials and produced unique results published in prominent journals; however, novel experimental studies inevitably experience setbacks.

During the process of becoming accustomed to the nude mouse model, we addressed numerous logistical challenges and practical problems. Nude mice are very delicate when exposed to physiological distress related to surgery. For example, a seemingly insignificant blood loss of only a few milliliters will endanger the ability of the animal to recover after surgery. Additionally, the lack of fur and

the chilling effect of a laminar airflow system result in drastic decreases in body temperature during extended operations.

We progressively learned how to deal with these issues using simple measures, including an improved injection technique for anesthesia induction and using bedding involving a heat pad during surgery, as well as increasing the room temperature from 20°C to 25°C. Moreover, we switched to gas anesthesia, which is more easily managed and less distressing for the animals.

Among the technical mistakes, cells were destroyed by the high printing pressure due to a cramped printing-head nozzle. In another experiment, batches of commercial cells (BM-MSCs) showed unexpectedly low viability and differentiation capacity, which nullified the experiment. We subsequently became more diligent in our choices of nozzles, and confirmation of stem cell viability prior to printing became a standard protocol.

Some studies offered surprises and unexpected results. For example, we hypothesized that some of the cells in central areas of the constructs would succumb to anoxia but were intrigued to detect no necrosis in any of the experiments. Instead, the cells survived and prospered without signs of distress. Furthermore, in study **III**, we were momentarily captivated by the distinct hot spots that suddenly emerged via MRI. The indisputable clarity of the contrast agent in the grid holes was beautiful, and the fact that this had never been seen before was astonishing. Equally satisfying were the distinct histomorphological patterns of GAGs distributed around each grid hole and corresponding to thriving chondrocytes at an ideal distance to maintain the correct oxygen tension.

6. Conclusions

We developed a 3D bioprinting methodology that demonstrates excellent biological compatibility and a high potential for clinical translation.

The primary results are as follows:

Study **I**: Human chondrocytes can be used for 3D bioprinting of cartilage-like constructs, and the presence of stem cells results in increasing chondrocyte proliferation.

Study **II**: Human cartilage-like constructs comprising chondrocytes and stem cells do not develop into bone, tumor, or connective tissue.

Study **III**: A gridded structure of the 3D-bioprinted construct allows ingrowth of blood vessels from the host, and NC/alginate-based bioink displays excellent diffusion characteristics.

Study **IV**: TNC demonstrates excellent biocompatibility.

7. Future perspectives

The goal of this thesis was to bring 3D bioprinting technology closer to clinical trials. Future goals include demonstrating the repeatability of the findings and further refinement of the methodology using an immunologically-competent animal model, such as porcine animal models, thereafter proceeding to human trials.

From a surgical standpoint, the reconstructive procedures should ideally be single-staged, safe, easily reproducible, and effective both functionally and cosmetically. From a legislative standpoint, the cell- and tissue-transplantation procedures must also adhere to good medical practice (GMP), as well as utilize approved technical equipment and environments throughout all of the steps.

GMP-certified 3D bioprinters and FDA-approved biomaterials are currently available for clinical use; however, the goal is to ensure quality throughout the entire process of reconstructive surgical treatments. We have assessed the Lipogems device, which mechanically disintegrates fat to yield a highly-pure lipoaspirate with a large percentage of ASCs (*46*). Recently, we evaluated another methodology to refine lipoaspirate via semi-automatic processing, enzymatic disintegration, washing, and centrifugation using the Cytori cell separator (*191*). In these studies, the resulting stem cell-rich SVF was further characterized and sorted using fluorescence-activated cell sorting to yield a potent population of ASCs that were then co-cultured with differentiated chondrocytes to create a suitable milieu for chondrocyte proliferation and cartilage tissue expansion. These studies are currently in the process of being submitted for publication.

Our observations identified the presence of vascular structures in fat assemblies within hours after implantation, and that functional circulation was presumably established in the following days. However, the details of this early vascularization process require further investigation.

Subsequent studies on cartilage tissue restoration will involve application of easily accessible ASCs rather than hBM-MSCs, as

ASCs reportedly yield a similar or possibly stronger boosting effect on chondrogenesis (*192-194*).

Future studies will focus on the use of animals harboring a competent immune system, such as a porcine model. Our findings suggest that the evaluated biomaterials are biologically inert and should, therefore, not induce an immune response. Moreover, the cells used in this methodology are autologous, unaltered, and undergo minimal handling. Additionally, we use no antibiotics and only enzymes during the cell-separation process. Nevertheless, a thorough assessment of this method requires its application in a model that closely mimics human-like physiology prior to human studies.

Furthermore, constructs with larger dimensions need to be evaluated using larger animal models in order to challenge diffusion limits. For example, use of a porcine model will allow implantation of constructs with increasing dimensions in the same animal in order to push the oxygenation boundaries.

8. Acknowledgments

I would like to express my sincere gratitude to the following individuals:

Professor **Lars Kölby**, my main supervisor, who has been indispensable to my completing this thesis. He has offered me tireless support and encouragement, as well as ingenious ideas and rock-solid scientific knowledge.

Associate professor **Stina Simonsson**, my assistant supervisor, who has been the source of vast biotechnological knowledge and invaluable assistance with the Cytori lipoaspirate procedures.

My second assistant supervisor and clinical colleague, **Karin Säljö**, for the never-ending discussions of science and her immense knowledge about stem cells and flow cytometry.

I would also like to acknowledge the following people for their contributions to the projects included in this thesis:

Paul Gatenholm, professor of chemical engineering at Chalmers and the director of the 3D Bioprinting Center. He initiated the collaboration between Chalmers and the Department of Plastic Surgery and has inspired all of us to continually think outside of the box.

My scientific co-worker, **Matteo Amoroso**, for great companionship during the exhausting animal experiments.

Anna Elander, Head of the Department of Plastic Surgery at Sahlgrenska University Hospital, for her encouragement, support, and prioritizing the time needed for research. Anna has also been my

leadership mentor for the last couple of years and an unwavering leader and role model.

My dear colleagues at the Department of Plastic Surgery, Sahlgrenska University Hospital, for making the daily work joyful and exciting.

Throughout the experiments, we have had access to the research facilities at the Department of Clinical Chemistry at Sahlgrenska University Hospital, the institution of Experimental Biomedicine at the University of Gothenburg, and specific analytical resources at the Department of Chemistry at the Chalmers University of Technology. For many of the complex analyses, we have had assistance from the many experts working with these specific procedures on a daily basis. I would like to specifically acknowledge the following individuals:

Camilla Brantsing provided me invaluable support with immunohistochemical analyses and image-scanning procedures.

Anders Lindahl, professor in clinical chemistry and the "cartilage maestro" at Sahlgrenska, for his extensive knowledge about everything related to cartilage.

Susann Li, the go-to person for flow cytometry experiments.

Mikael Montelius, the radiation physicist who performed all of the MRI sessions, post-processing, and data interpretation for study **III**.

Johan Mölne, senior pathologist at the Department of Pathology at Sahlgrenska, for his expert contributions to and enthusiasm for study **IV**.

Linnéa Stridh Orrhult, **Kajsa Markstedt**, and **Sanna Sämfors** who co-authored the studies and performed the 3D bioprinting procedures, as well as the biomaterial analyses.

Mona Engström, who performed some of the immunohistochemical analyses in study **III**.

Emman Shubar for all her support with the logistics and practical arrangements necessary for the animal experiments.

Inger Ögärd, who helped us with the FISH analyses in study **I**.

Dr. **Katharina Stölzel**, who provided the cartilage samples.

Dr. **Silke Schwartz** and Prof. Dr. **Gundula Schulze-Tanzil**, who performed the cell-isolation and cultivation procedures in study **III**.

The plastic surgeons and nurses at **Art Clinic** who always greeted me with enthusiasm and provided the lipoaspirate for the research projects.

I would not have made it through this process without my beloved wife **Linda** and two wonderful sons, **Axel** and **Arvid**, who were my sources of strength and resilience throughout this scientific endeavor. They have provided me with a solid foundation, support, and relentless encouragement in good times and bad.

My mother, **Lisbeth**, and my father, **Göran**, for their never-ending support and belief.

Mats Hulander, a brilliant scientist and my closest friend since childhood. After hours of scientific discussions, he is still curious and enthusiastic. Anything Mats does not already know about nanostructured surfaces, butterflies, the Baikal oilfish, drone photography, the Fender Rhodes piano, and laser pointers is simply not worth knowing.

Finally, I would like to acknowledge the following patrons:

The Ann-Mari and Per Ahlquists Foundation for long-term financial support.

The Gothenburg Medical Society for a 4-month scholarship, as well as travel grants that enabled my attendance of international conferences.

The research projects were also financed by grants to professor Lars Kölby from **Vetenskapsrådet** (2021-00971) and grants from the **Swedish State** under the agreement between the government and the county councils: the ALF-agreement (ALFGBG-716621 and ALFGBG-965533).

9. References

1. H. Kodama, Automatic method for fabricating a three-dimensional plastic model with photo-hardening polymer. *Review of Scientific Instruments* **52**, 1770 (1981).
2. C. W. Hull, Apparatus for production of three-dimensional objects by stereolithography. *U.S. patent US4575330 A*, (1986).
3. G. Forgacs, N. S. Jaikaria, H. L. Frisch, S. A. Newman, Wetting, percolation and morphogenesis in a model tissue system. *J Theor Biol* **140**, 417-430 (1989).
4. F. Oberpenning, J. Meng, J. J. Yoo, A. Atala, De novo reconstitution of a functional mammalian urinary bladder by tissue engineering. *Nat Biotechnol* **17**, 149-155 (1999).
5. V. Mironov, T. Boland, T. Trusk, G. Forgacs, R. R. Markwald, Organ printing: computer-aided jet-based 3D tissue engineering. *Trends Biotechnol* **21**, 157-161 (2003).
6. A. Cui, H. Li, D. Wang, J. Zhong, Y. Chen, H. Lu, Global, regional prevalence, incidence and risk factors of knee osteoarthritis in population-based studies. *EClinicalMedicine* **29-30**, 100587 (2020).
7. L. Peterson, H. S. Vasiliadis, M. Brittberg, A. Lindahl, Autologous chondrocyte implantation: a long-term follow-up. *Am J Sports Med* **38**, 1117-1124 (2010).
8. M. Brittberg, A. Lindahl, A. Nilsson, C. Ohlsson, O. Isaksson, L. Peterson, Treatment of deep cartilage defects in the knee with autologous chondrocyte transplantation. *N Engl J Med* **331**, 889-895 (1994).
9. G. Knutsen, L. Engebretsen, T. C. Ludvigsen, J. O. Drogset, T. Grontvedt, E. Solheim, T. Strand, S. Roberts, V. Isaksen, O. Johansen, Autologous chondrocyte implantation compared with microfracture in the knee. A randomized trial. *J Bone Joint Surg Am* **86**, 455-464 (2004).
10. Y. Jiang, Y. Cai, W. Zhang, Z. Yin, C. Hu, T. Tong, P. Lu, S. Zhang, D. Neculai, R. S. Tuan, H. W. Ouyang, Human Cartilage-Derived Progenitor Cells From Committed Chondrocytes for Efficient Cartilage Repair and Regeneration. *Stem Cells Transl Med* **5**, 733-744 (2016).
11. Z. Jian, T. Zhuang, T. Qinyu, P. Liqing, L. Kun, L. Xujiang, W. Diaodiao, Y. Zhen, J. Shuangpeng, S. Xiang, H. Jingxiang, L. Shuyun, H. Libo, T. Peifu, Y. Qi, G. Quanyi, 3D bioprinting of a biomimetic meniscal scaffold for application in tissue engineering. *Bioact Mater* **6**, 1711-1726 (2021).
12. P. Thavaneswaran, M. Vandepeer, Lumbar artificial intervertebral disc replacement: a systematic review. *ANZ J Surg* **84**, 121-127 (2014).

13. R. D. Bowles, R. M. Williams, W. R. Zipfel, L. J. Bonassar, Self-assembly of aligned tissue-engineered annulus fibrosus and intervertebral disc composite via collagen gel contraction. *Tissue Eng Part A* **16**, 1339-1348 (2010).
14. L. J. Smith, J. A. Chiaro, N. L. Nerurkar, D. H. Cortes, S. D. Horava, N. M. Hebela, R. L. Mauck, G. R. Dodge, D. M. Elliott, Nucleus pulposus cells synthesize a functional extracellular matrix and respond to inflammatory cytokine challenge following long-term agarose culture. *Eur Cell Mater* **22**, 291-301 (2011).
15. T. Ganey, J. Libera, V. Moos, O. Alasevic, K. G. Fritsch, H. J. Meisel, W. C. Hutton, Disc chondrocyte transplantation in a canine model: a treatment for degenerated or damaged intervertebral disc. *Spine (Phila Pa 1976)* **28**, 2609-2620 (2003).
16. H. J. Meisel, V. Siodla, T. Ganey, Y. Minkus, W. C. Hutton, O. J. Alasevic, Clinical experience in cell-based therapeutics: disc chondrocyte transplantation A treatment for degenerated or damaged intervertebral disc. *Biomol Eng* **24**, 5-21 (2007).
17. T. Graf, Differentiation plasticity of hematopoietic cells. *Blood* **99**, 3089-3101 (2002).
18. D. Sakai, J. Mochida, Y. Yamamoto, T. Nomura, M. Okuma, K. Nishimura, T. Nakai, K. Ando, T. Hotta, Transplantation of mesenchymal stem cells embedded in Atelocollagen gel to the intervertebral disc: a potential therapeutic model for disc degeneration. *Biomaterials* **24**, 3531-3541 (2003).
19. D. Wu, J. Tan, L. Yao, J. Tian, B. Luo, L. Li, C. Zhou, L. Lu, Customized composite intervertebral disc scaffolds by integrated 3D bioprinting for therapeutic implantation. *Composites Part A: Applied Science and Manufacturing* **147**, 106468 (2021).
20. R. Gaebel, N. Ma, J. Liu, J. Guan, L. Koch, C. Klopsch, M. Gruene, A. Toelk, W. Wang, P. Mark, F. Wang, B. Chichkov, W. Li, G. Steinhoff, Patterning human stem cells and endothelial cells with laser printing for cardiac regeneration. *Biomaterials* **32**, 9218-9230 (2011).
21. B. Duan, E. Kapetanovic, L. A. Hockaday, J. T. Butcher, Three-dimensional printed trileaflet valve conduits using biological hydrogels and human valve interstitial cells. *Acta Biomater* **10**, 1836-1846 (2014).
22. P. Wang, X. Li, W. Zhu, Z. Zhong, A. Moran, W. Wang, K. Zhang, C. Shaochen, 3D bioprinting of hydrogels for retina cell culturing. *Bioprinting* **11**, (2018).
23. A. Faulkner-Jones, C. Fyfe, D. J. Cornelissen, J. Gardner, J. King, A. Courtney, W. Shu, Bioprinting of human pluripotent stem cells and their directed differentiation into hepatocyte-like cells for the generation of mini-livers in 3D. *Biofabrication* **7**, 044102 (2015).
24. X. Ma, X. Qu, W. Zhu, Y. S. Li, S. Yuan, H. Zhang, J. Liu, P. Wang, C. S. Lai, F. Zanella, G. S. Feng, F. Sheikh, S. Chien, S. Chen, Deterministically patterned biomimetic human iPSC-derived hepatic

model via rapid 3D bioprinting. *Proc Natl Acad Sci U S A* **113**, 2206-2211 (2016).
25. K. Han, J. Kim, D. Son, B. Park, How to harvest the maximal amount of conchal cartilage grafts. *J Plast Reconstr Aesthet Surg* **61**, 1465-1471 (2008).
26. M. G.L., Auricular cartilage grafts and nasal surgery. *Laryngoscope* **114**, 2092-2101 (2004).
27. S. Nagata, A new method of total reconstruction of the auricle for microtia. *Plast Reconstr Surg* **92**, 187-201 (1993).
28. B. Brent, The correction of mi-rotia with autogenous cartilage grafts: I. The classic deformity.? *Plast Reconstr Surg* **66**, 1-12 (1980).
29. B. Brent, The correction of microtia with autogenous cartilage grafts: II. Atypical and complex deformities. *Plast Reconstr Surg* **66**, 13-21 (1980).
30. M. S. T. Mau T., Kim D.W., Cadaveric and engineering analysis of the septal L-strut. *Laryngoscope* **117**, 1902-1906 (2007).
31. E. K. K. Kim D.W., O'Grady K., Biomechanical strength of human nasal septal lining: A comparison of the constituent layers. *Laryngoscope* **115**, 1451-1453 (2005).
32. Y. Kawanabe, S. Nagata, A new method of costal cartilage harvest for total auricular reconstruction: part I. Avoidance and prevention of intraoperative and postoperative complications and problems. *Plast Reconstr Surg* **117**, 2011-2018 (2006).
33. K. Ohara, K. Nakamura, E. Ohta, Chest wall deformities and thoracic scoliosis after costal cartilage graft harvesting. *Plast Reconstr Surg* **99**, 1030-1036 (1997).
34. Y. Kawanabe, S. Nagata, A new method of costal cartilage harvest for total auricular reconstruction: part II. Evaluation and analysis of the regenerated costal cartilage. *Plast Reconstr Surg* **119**, 308-315 (2007).
35. F. Firmin, A. Marchac, A novel algorithm for autologous ear reconstruction. *Semin Plast Surg* **25**, 257-264 (2011).
36. A. Tjellstrom, J. Lindstrom, O. Hallen, T. Albrektsson, P. I. Branemark, Osseointegrated titanium implants in the temporal bone. A clinical study on bone-anchored hearing aids. *Am J Otol* **2**, 304-310 (1981).
37. G. H. Wilkes, J. F. Wolfaardt, Osseointegrated alloplastic versus autogenous ear reconstruction: criteria for treatment selection. *Plast Reconstr Surg* **93**, 967-979 (1994).
38. K. M. Holgers, A. Tjellstrom, L. M. Bjursten, B. E. Erlandsson, Soft tissue reactions around percutaneous implants: a clinical study on skin-penetrating titanium implants used for bone-anchored auricular prostheses. *Int J Oral Maxillofac Implants* **2**, 35-39 (1987).
39. T. Westin, A. Tjellstrom, E. Hammerlid, K. Bergstrom, B. Rangert, Long-term study of quality and safety of osseointegration for the retention of auricular prostheses. *Otolaryngol Head Neck Surg* **121**, 133-143 (1999).

40. L. J. Korus, J. N. Wong, G. H. Wilkes, Long-term follow-up of osseointegrated auricular reconstruction. *Plast Reconstr Surg* **127**, 630-636 (2011).
41. A. K. Gundestrup, C. D. Lynggaard, L. Forner, T. J. Heino, K. K. Jakobsen, A. Fischer-Nielsen, C. Gronhoj, C. von Buchwald, Mesenchymal Stem Cell Therapy for Osteoradionecrosis of the Mandible: a Systematic Review of Preclinical and Human Studies. *Stem Cell Rev Rep* **16**, 1208-1221 (2020).
42. Z. Aytac, N. Dubey, A. Daghrery, J. A. Ferreira, I. J. D. Araujo, M. Castilho, J. Malda, M. C. Bottino, Innovations in craniofacial bone and periodontal tissue engineering - from electrospinning to converged biofabrication. *Int Mater Rev*, (2021).
43. F. Pati, D. H. Ha, J. Jang, H. H. Han, J. W. Rhie, D. W. Cho, Biomimetic 3D tissue printing for soft tissue regeneration. *Biomaterials* **62**, 164-175 (2015).
44. W. W. Cho, B. S. Kim, M. Ahn, Y. H. Ryu, D. H. Ha, J. S. Kong, J. W. Rhie, D. W. Cho, Flexible Adipose-Vascular Tissue Assembly Using Combinational 3D Printing for Volume-Stable Soft Tissue Reconstruction. *Adv Healthc Mater* **10**, e2001693 (2021).
45. M. Amoroso, P. Apelgren, K. Säljö, M. Montelius, L. S. Orrhult, M. Engström, P. Gatenholm, L. Kölby, Functional and morphological studies of in vivo vascularization of 3D-bioprinted human fat grafts. *Bioprinting* **23**, (2021).
46. K. Säljö, L. S. Orrhult, P. Apelgren, K. Markstedt, L. Kölby, P. Gatenholm, Successful engraftment, vascularization, and In vivo survival of 3D-bioprinted human lipoaspirate-derived adipose tissue. *Bioprinting* **17**, (2020).
47. L. Groening, L. D. Holthuis, S. Polesie, H. H. Sonnergren, Clinical Outcomes of Punch-grafting for Chronic Leg and Foot Ulcers: A Retrospective Non-comparative Cohort Study. *Acta Derm Venereol* **97**, 131-132 (2017).
48. S. Lönnqvist, J. Rakar, K. Briheim, G. Kratz, Biodegradable Gelatin Microcarriers Facilitate Re-Epithelialization of Human Cutaneous Wounds - An In Vitro Study in Human Skin. *PloS one* **10**, e0128093-e0128093 (2015).
49. M. Hosseini, A. Shafiee, Engineering Bioactive Scaffolds for Skin Regeneration. *Small (Weinheim an der Bergstrasse, Germany)* **17**, 2101384-n/a (2021).
50. L. K. Branski, D. N. Herndon, C. Pereira, R. P. Mlcak, M. M. Celis, J. O. Lee, A. P. Sanford, W. B. Norbury, X.-J. Zhang, M. G. Jeschke, Longitudinal assessment of Integra in primary burn management: A randomized pediatric clinical trial. *Critical care medicine* **35**, 2615-2623 (2007).
51. H. Lagus, M. Sarlomo-Rikala, T. Böhling, J. Vuola, Prospective study on burns treated with Integra®, a cellulose sponge and split thickness skin graft: comparative clinical and histological study--randomized

controlled trial. *Burns : journal of the International Society for Burn Injuries* **39**, 1577-1587 (2013).
52. C. E. Hart, A. Loewen-Rodriguez, J. Lessem, Dermagraft: Use in the Treatment of Chronic Wounds. *Adv Wound Care (New Rochelle)* **1**, 138-141 (2012).
53. T. Weng, W. Zhang, Y. Xia, P. Wu, M. Yang, R. Jin, S. Xia, J. Wang, C. You, C. Han, X. Wang, 3D bioprinting for skin tissue engineering: Current status and perspectives. *Journal of tissue engineering* **12**, 204173142110285-20417314211028574 (2021).
54. J. W. Alford, B. J. Cole, Cartilage restoration, part 1: basic science, historical perspective, patient evaluation, and treatment options. *Am J Sports Med* **33**, 295-306 (2005).
55. K. Bobacz, L. Erlacher, J. Smolen, A. Soleiman, W. B. Graninger, Chondrocyte number and proteoglycan synthesis in the aging and osteoarthritic human articular cartilage. *Ann Rheum Dis* **63**, 1618-1622 (2004).
56. R. A. Stockwell, Chondrocytes. *J Clin Pathol Suppl (R Coll Pathol)* **12**, 7-13 (1978).
57. H. K. Gahunia, Pritzker, K.P.H., in *Articular Cartilage of the Knee. ,* G. A. Gahunia H., Pritzker K., Babyn P., Murnaghan L., Ed. (Springer, New York, NY., 2020).
58. J. Li, S. Dong, The Signaling Pathways Involved in Chondrocyte Differentiation and Hypertrophic Differentiation. *Stem Cells Int* **2016**, 2470351 (2016).
59. M. J. Zuscik, M. J. Hilton, X. Zhang, D. Chen, R. J. O'Keefe, Regulation of chondrogenesis and chondrocyte differentiation by stress. *J Clin Invest* **118**, 429-438 (2008).
60. A. Augello, C. De Bari, The regulation of differentiation in mesenchymal stem cells. *Hum Gene Ther* **21**, 1226-1238 (2010).
61. Y. Takigawa, K. Hata, S. Muramatsu, K. Amano, K. Ono, M. Wakabayashi, A. Matsuda, K. Takada, R. Nishimura, T. Yoneda, The transcription factor Znf219 regulates chondrocyte differentiation by assembling a transcription factory with Sox9. *J Cell Sci* **123**, 3780-3788 (2010).
62. G. Zhou, Q. Zheng, F. Engin, E. Munivez, Y. Chen, E. Sebald, D. Krakow, B. Lee, Dominance of SOX9 function over RUNX2 during skeletogenesis. *Proc Natl Acad Sci U S A* **103**, 19004-19009 (2006).
63. K. Hata, Y. Takahata, T. Murakami, R. Nishimura, Transcriptional Network Controlling Endochondral Ossification. *J Bone Metab* **24**, 75-82 (2017).
64. D. Duprez, E. J. Bell, M. K. Richardson, C. W. Archer, L. Wolpert, P. M. Brickell, P. H. Francis-West, Overexpression of BMP-2 and BMP-4 alters the size and shape of developing skeletal elements in the chick limb. *Mech Dev* **57**, 145-157 (1996).
65. P. Guo, Z. L. Shi, A. Liu, T. Lin, F. Bi, M. Shi, S. G. Yan, Effects of cartilage oligomeric matrix protein on bone morphogenetic protein-2-

induced differentiation of mesenchymal stem cells. *Orthop Surg* **6**, 280-287 (2014).
66. T.-J. Lee, J. Jang, S. Kang, M. Jin, H. Shin, D.-W. Kim, B.-S. Kim, Enhancement of osteogenic and chondrogenic differentiation of human embryonic stem cells by mesodermal lineage induction with BMP-4 and FGF2 treatment. *Biochemical and biophysical research communications* **430**, 793-797 (2013).
67. T. S. de Windt, J. A. Hendriks, X. Zhao, L. A. Vonk, L. B. Creemers, W. J. Dhert, M. A. Randolph, D. B. Saris, Concise review: unraveling stem cell cocultures in regenerative medicine: which cell interactions steer cartilage regeneration and how? *Stem Cells Transl Med* **3**, 723-733 (2014).
68. C. Phornphutkul, K. Y. Wu, X. Yang, Q. Chen, P. A. Gruppuso, Insulin-like growth factor-I signaling is modified during chondrocyte differentiation. *J Endocrinol* **183**, 477-486 (2004).
69. S. Stricker, R. Fundele, A. Vortkamp, S. Mundlos, Role of Runx genes in chondrocyte differentiation. *Dev Biol* **245**, 95-108 (2002).
70. R. Nishimura, K. Hata, Y. Takahata, T. Murakami, E. Nakamura, H. Yagi, Regulation of Cartilage Development and Diseases by Transcription Factors. *J Bone Metab* **24**, 147-153 (2017).
71. P. Apelgren, E. Karabulut, M. Amoroso, A. Mantas, H. Martínez Ávila, L. Kölby, T. Kondo, G. Toriz, P. Gatenholm, In Vivo Human Cartilage Formation in Three-Dimensional Bioprinted Constructs with a Novel Bacterial Nanocellulose Bioink. *ACS Biomaterials Science and Engineering* **5**, 2482-2490 (2019).
72. M. S. Lee, M. J. Stebbins, H. Jiao, H. C. Huang, E. M. Leiferman, B. E. Walczak, S. P. Palecek, E. V. Shusta, W. J. Li, Comparative evaluation of isogenic mesodermal and ectomesodermal chondrocytes from human iPSCs for cartilage regeneration. *Sci Adv* **7**, (2021).
73. C. T. Brighton, R. B. Heppenstall, Oxygen tension in zones of the epiphyseal plate, the metaphysis and diaphysis. An in vitro and in vivo study in rats and rabbits. *J Bone Joint Surg Am* **53**, 719-728 (1971).
74. R. Rajpurohit, C. J. Koch, Z. Tao, C. M. Teixeira, I. M. Shapiro, Adaptation of chondrocytes to low oxygen tension: relationship between hypoxia and cellular metabolism. *J Cell Physiol* **168**, 424-432 (1996).
75. S. Saini, T. M. Wick, Effect of low oxygen tension on tissue-engineered cartilage construct development in the concentric cylinder bioreactor. *Tissue Eng* **10**, 825-832 (2004).
76. K. Scherer, M. Schunke, R. Sellckau, J. Hassenpflug, B. Kurz, The influence of oxygen and hydrostatic pressure on articular chondrocytes and adherent bone marrow cells in vitro. *Biorheology* **41**, 323-333 (2004).
77. N. Schneider, A. Mouithys-Mickalad, J. P. Lejeune, C. Duyckaerts, F. Sluse, G. Deby-Dupont, D. Serteyn, Oxygen consumption of equine articular chondrocytes: Influence of applied oxygen tension and glucose concentration during culture. *Cell Biol Int* **31**, 878-886 (2007).

78. B. Cao, Z. Li, R. Peng, J. Ding, Effects of cell-cell contact and oxygen tension on chondrogenic differentiation of stem cells. *Biomaterials* **64**, 21-32 (2015).
79. C. L. Murphy, J. M. Polak, Control of human articular chondrocyte differentiation by reduced oxygen tension. *J Cell Physiol* **199**, 451-459 (2004).
80. A. J. Sophia Fox, A. Bedi, S. A. Rodeo, The basic science of articular cartilage: structure, composition, and function. *Sports Health* **1**, 461-468 (2009).
81. M. J. Lammi, J. Piltti, J. Prittinen, C. Qu, Challenges in Fabrication of Tissue-Engineered Cartilage with Correct Cellular Colonization and Extracellular Matrix Assembly. *Int J Mol Sci* **19**, (2018).
82. Z. Wang, Z. Li, Z. Li, B. Wu, Y. Liu, W. Wu, Cartilaginous extracellular matrix derived from decellularized chondrocyte sheets for the reconstruction of osteochondral defects in rabbits. *Acta Biomaterialia* **81**, 129-145 (2018).
83. T. S. de Windt, D. B. Saris, I. C. Slaper-Cortenbach, M. H. van Rijen, D. Gawlitta, L. B. Creemers, R. A. de Weger, W. J. Dhert, L. A. Vonk, Direct Cell-Cell Contact with Chondrocytes Is a Key Mechanism in Multipotent Mesenchymal Stromal Cell-Mediated Chondrogenesis. *Tissue Eng Part A* **21**, 2536-2547 (2015).
84. E. J. Levorson, M. Santoro, F. K. Kasper, A. G. Mikos, Direct and indirect co-culture of chondrocytes and mesenchymal stem cells for the generation of polymer/extracellular matrix hybrid constructs. *Acta Biomater* **10**, 1824-1835 (2014).
85. Q. Zuo, W. Cui, F. Liu, Q. Wang, Z. Chen, W. Fan, Co-cultivated mesenchymal stem cells support chondrocytic differentiation of articular chondrocytes. *Int Orthop* **37**, 747-752 (2013).
86. Y. Park, S. T. Ji, U. Yong, S. Das, W. B. Jang, G. Ahn, S. M. Kwon, J. Jang, 3D bioprinted tissue-specific spheroidal multicellular microarchitectures for advanced cell therapy. *Biofabrication* **13**, (2021).
87. L. De Moor, E. Beyls, H. Declercq, Scaffold Free Microtissue Formation for Enhanced Cartilage Repair. *Ann Biomed Eng* **48**, 298-311 (2020).
88. S. Wakao, Y. Kuroda, F. Ogura, T. Shigemoto, M. Dezawa, Regenerative Effects of Mesenchymal Stem Cells: Contribution of Muse Cells, a Novel Pluripotent Stem Cell Type that Resides in Mesenchymal Cells. *Cells* **1**, 1045-1060 (2012).
89. V. Sengupta, S. Sengupta, A. Lazo, P. Woods, A. Nolan, N. Bremer, Exosomes Derived from Bone Marrow Mesenchymal Stem Cells as Treatment for Severe COVID-19. *Stem Cells Dev* **29**, 747-754 (2020).
90. R. Madonna, D. A. Taylor, Y. J. Geng, R. De Caterina, H. Shelat, E. C. Perin, J. T. Willerson, Transplantation of mesenchymal cells rejuvenated by the overexpression of telomerase and myocardin promotes revascularization and tissue repair in a murine model of hindlimb ischemia. *Circ Res* **113**, 902-914 (2013).

91. B. Gharibi, S. Farzadi, M. Ghuman, F. J. Hughes, Inhibition of Akt/mTOR attenuates age-related changes in mesenchymal stem cells. *Stem Cells* **32**, 2256-2266 (2014).
92. A. Uccelli, L. Moretta, V. Pistoia, Mesenchymal stem cells in health and disease. *Nat Rev Immunol* **8**, 726-736 (2008).
93. Q. Lian, Y. Zhang, X. Liang, F. Gao, H. F. Tse, Directed Differentiation of Human-Induced Pluripotent Stem Cells to Mesenchymal Stem Cells. *Methods Mol Biol* **1416**, 289-298 (2016).
94. A. R. Williams, J. M. Hare, Mesenchymal stem cells: biology, pathophysiology, translational findings, and therapeutic implications for cardiac disease. *Circ Res* **109**, 923-940 (2011).
95. J. M. Brunger, A. Zutshi, V. P. Willard, C. A. Gersbach, F. Guilak, CRISPR/Cas9 Editing of Murine Induced Pluripotent Stem Cells for Engineering Inflammation-Resistant Tissues. *Arthritis Rheumatol* **69**, 1111-1121 (2017).
96. D. Mieth, Going to the roots of the stem cell debate - The ethical problems of using embryos for research. *Embo Rep* **1**, 4-6 (2000).
97. M. Yoshihara, Y. Hayashizaki, Y. Murakawa, Genomic Instability of iPSCs: Challenges Towards Their Clinical Applications. *Stem Cell Rev Rep* **13**, 7-16 (2017).
98. M. Yoshihara, A. Oguchi, Y. Murakawa, Genomic Instability of iPSCs and Challenges in Their Clinical Applications. *Adv Exp Med Biol* **1201**, 23-47 (2019).
99. P. Hou, Y. Li, X. Zhang, C. Liu, J. Guan, H. Li, T. Zhao, J. Ye, W. Yang, K. Liu, J. Ge, J. Xu, Q. Zhang, Y. Zhao, H. Deng, Pluripotent stem cells induced from mouse somatic cells by small-molecule compounds. *Science* **341**, 651-654 (2013).
100. T. Wang, P. Nimkingratana, C. A. Smith, A. Cheng, T. E. Hardingham, S. J. Kimber, Enhanced chondrogenesis from human embryonic stem cells. *Stem Cell Res* **39**, 101497 (2019).
101. M. Bami, T. Sarlikiotis, M. Milonaki, M. Vikentiou, E. Konsta, V. Kapsimali, V. Pappa, D. Koulalis, E. O. Johnson, P. N. Soucacos, Superiority of synovial membrane mesenchymal stem cells in chondrogenesis, osteogenesis, myogenesis and tenogenesis in a rabbit model. *Injury* **51**, 2855-2865 (2020).
102. P. A. Zuk, M. Zhu, H. Mizuno, J. Huang, J. W. Futrell, A. J. Katz, P. Benhaim, H. P. Lorenz, M. H. Hedrick, Multilineage cells from human adipose tissue: implications for cell-based therapies. *Tissue Eng* **7**, 211-228 (2001).
103. B. A. Bunnell, M. Flaat, C. Gagliardi, B. Patel, C. Ripoll, Adipose-derived stem cells: isolation, expansion and differentiation. *Methods* **45**, 115-120 (2008).
104. M. Locke, J. Windsor, P. R. Dunbar, Human adipose-derived stem cells: isolation, characterization and applications in surgery. *ANZ J Surg* **79**, 235-244 (2009).

105. K. McIntosh, S. Zvonic, S. Garrett, J. B. Mitchell, Z. E. Floyd, L. Hammill, A. Kloster, Y. Di Halvorsen, J. P. Ting, R. W. Storms, B. Goh, G. Kilroy, X. Wu, J. M. Gimble, The immunogenicity of human adipose-derived cells: temporal changes in vitro. *Stem Cells* **24**, 1246-1253 (2006).
106. K. R. McIntosh, T. Frazier, B. G. Rowan, J. M. Gimble, Evolution and future prospects of adipose-derived immunomodulatory cell therapeutics. *Expert Rev Clin Immunol* **9**, 175-184 (2013).
107. J. C. Brown, H. Shang, Y. Li, N. Yang, N. Patel, A. J. Katz, Isolation of Adipose-Derived Stromal Vascular Fraction Cells Using a Novel Point-of-Care Device: Cell Characterization and Review of the Literature. *Tissue Eng Part C Methods* **23**, 125-135 (2017).
108. K. C. Hicok, M. H. Hedrick, Automated isolation and processing of adipose-derived stem and regenerative cells. *Methods Mol Biol* **702**, 87-105 (2011).
109. J. R. Garza, R. E. Campbell, F. P. Tjoumakaris, K. B. Freedman, L. S. Miller, D. Santa Maria, B. S. Tucker, Clinical Efficacy of Intra-articular Mesenchymal Stromal Cells for the Treatment of Knee Osteoarthritis: A Double-Blinded Prospective Randomized Controlled Clinical Trial. *Am J Sports Med* **48**, 588-598 (2020).
110. J. Bukowska, A. Alarcon Uquillas, X. Wu, T. Frazier, K. Walendzik, M. Vanek, D. Gaupp, B. A. Bunnell, P. Kosnik, B. Mehrara, A. J. Katz, B. Gawronska-Kozak, J. M. Gimble, Safety and Efficacy of Human Adipose-Derived Stromal/Stem Cell Therapy in an Immunocompetent Murine Pressure Ulcer Model. *Stem Cells Dev* **29**, 440-451 (2020).
111. A. Casado-Diaz, J. M. Quesada-Gomez, G. Dorado, Extracellular Vesicles Derived From Mesenchymal Stem Cells (MSC) in Regenerative Medicine: Applications in Skin Wound Healing. *Front Bioeng Biotechnol* **8**, 146 (2020).
112. A. Gowen, F. Shahjin, S. Chand, K. E. Odegaard, S. V. Yelamanchili, Mesenchymal Stem Cell-Derived Extracellular Vesicles: Challenges in Clinical Applications. *Front Cell Dev Biol* **8**, 149 (2020).
113. S. Ren, J. Chen, D. Duscher, Y. Liu, G. Guo, Y. Kang, H. Xiong, P. Zhan, Y. Wang, C. Wang, H. G. Machens, Z. Chen, Microvesicles from human adipose stem cells promote wound healing by optimizing cellular functions via AKT and ERK signaling pathways. *Stem Cell Res Ther* **10**, 47 (2019).
114. C. J. Poon, E. C. M. V. Pereira, S. Sinha, J. A. Palmer, A. A. Woods, W. A. Morrison, K. M. Abberton, Preparation of an adipogenic hydrogel from subcutaneous adipose tissue. *Acta Biomater* **9**, 5609-5620 (2013).
115. O. A. Mohiuddin, B. Campbell, J. N. Poche, M. Ma, E. Rogers, D. Gaupp, M. A. A. Harrison, B. A. Bunnell, D. J. Hayes, J. M. Gimble, Decellularized Adipose Tissue Hydrogel Promotes Bone Regeneration in Critical-Sized Mouse Femoral Defect Model. *Front Bioeng Biotechnol* **7**, 211 (2019).

116. C. D. O'Connell, C. Di Bella, F. Thompson, C. Augustine, S. Beirne, R. Cornock, C. J. Richards, J. Chung, S. Gambhir, Z. L. Yue, J. Bourke, B. B. Zhang, A. Taylor, A. Quigley, R. Kapsa, P. Choong, G. G. Wallace, Development of the Biopen: a handheld device for surgical printing of adipose stem cells at a chondral wound site. *Biofabrication* **8**, (2016).
117. Y. Jang, Y. G. Koh, Y. J. Choi, S. H. Kim, D. S. Yoon, M. Lee, J. W. Lee, Characterization of adipose tissue-derived stromal vascular fraction for clinical application to cartilage regeneration. *In Vitro Cell Dev Biol Anim* **51**, 142-150 (2015).
118. L. Wu, H. J. Prins, J. Leijten, M. N. Helder, D. Evseenko, L. Moroni, C. A. van Blitterswijk, Y. Lin, M. Karperien, Chondrocytes Cocultured with Stromal Vascular Fraction of Adipose Tissue Present More Intense Chondrogenic Characteristics Than with Adipose Stem Cells. *Tissue Eng Part A* **22**, 336-348 (2016).
119. W. J. Jurgens, A. van Dijk, B. Z. Doulabi, F. B. Niessen, M. J. Ritt, F. J. van Milligen, M. N. Helder, Freshly isolated stromal cells from the infrapatellar fat pad are suitable for a one-step surgical procedure to regenerate cartilage tissue. *Cytotherapy* **11**, 1052-1064 (2009).
120. Z. Hong, J. Chen, S. Zhang, C. Zhao, M. Bi, X. Chen, Q. Bi, Intra-articular injection of autologous adipose-derived stromal vascular fractions for knee osteoarthritis: a double-blind randomized self-controlled trial. *Int Orthop* **43**, 1123-1134 (2019).
121. F. Bianchi, M. Maioli, E. Leonardi, E. Olivi, G. Pasquinelli, S. Valente, A. J. Mendez, C. Ricordi, M. Raffaini, C. Tremolada, C. Ventura, A new nonenzymatic method and device to obtain a fat tissue derivative highly enriched in pericyte-like elements by mild mechanical forces from human lipoaspirates. *Cell Transplantation* **22**, 2063-2077 (2013).
122. C. Tremolada, V. Colombo, C. Ventura, Adipose Tissue and Mesenchymal Stem Cells: State of the Art and Lipogems® Technology Development. *Current Stem Cell Reports* **2**, 304-312 (2016).
123. M. Minelli, M. G. Baschetti, F. Doghieri, M. Ankerfors, T. Lindstrom, I. Siro, D. Plackett, Investigation of mass transport properties of microfibrillated cellulose (MFC) films. *J Membrane Sci* **358**, 67-75 (2010).
124. A. Miettinen, G. Chinga-Carrasco, M. Kataja, Three-dimensional microstructural properties of nanofibrillated cellulose films. *Int J Mol Sci* **15**, 6423-6440 (2014).
125. A. Cochis, S. Grad, M. J. Stoddart, S. Fare, L. Altomare, B. Azzimonti, M. Alini, L. Rimondini, Bioreactor mechanically guided 3D mesenchymal stem cell chondrogenesis using a biocompatible novel thermo-reversible methylcellulose-based hydrogel. *Sci Rep* **7**, 45018 (2017).
126. N. Contessi, L. Altomare, A. Filipponi, S. Fare, Thermo-responsive properties of methylcellulose hydrogels for cell sheet engineering. *Mater Lett* **207**, 157-160 (2017).

127. M. Smyth, C. Fournier, C. Driemeier, C. Picart, E. J. Foster, J. Bras, Tunable Structural and Mechanical Properties of Cellulose Nanofiber Substrates in Aqueous Conditions for Stem Cell Culture. *Biomacromolecules* **18**, 2034-2044 (2017).
128. J. S. Gonzalez, L. N. Luduena, A. Ponce, V. A. Alvarez, Poly(vinyl alcohol)/cellulose nanowhiskers nanocomposite hydrogels for potential wound dressings. *Mater Sci Eng C Mater Biol Appl* **34**, 54-61 (2014).
129. Y. Li, S. Wang, R. Huang, Z. Huang, B. Hu, W. Zheng, G. Yang, X. Jiang, Evaluation of the effect of the structure of bacterial cellulose on full thickness skin wound repair on a microfluidic chip. *Biomacromolecules* **16**, 780-789 (2015).
130. F. Sun, H. R. Nordli, B. Pukstad, E. Kristofer Gamstedt, G. Chinga-Carrasco, Mechanical characteristics of nanocellulose-PEG bionanocomposite wound dressings in wet conditions. *J Mech Behav Biomed Mater* **69**, 377-384 (2017).
131. T. Hakkarainen, R. Koivuniemi, M. Kosonen, C. Escobedo-Lucea, A. Sanz-Garcia, J. Vuola, J. Valtonen, P. Tammela, A. Makitie, K. Luukko, M. Yliperttula, H. Kavola, Nanofibrillar cellulose wound dressing in skin graft donor site treatment. *J Control Release* **244**, 292-301 (2016).
132. E. Vatankhah, M. P. Prabhakaran, G. Jin, L. G. Mobarakeh, S. Ramakrishna, Development of nanofibrous cellulose acetate/gelatin skin substitutes for variety wound treatment applications. *J Biomater Appl* **28**, 909-921 (2014).
133. J. D. P. de Amorim, K. C. de Souza, C. R. Duarte, I. D. Duarte, F. D. S. Ribeiro, G. S. Silva, P. M. A. de Farias, A. Stingl, A. F. S. Costa, G. M. Vinhas, L. A. Sarubbo, Plant and bacterial nanocellulose: production, properties and applications in medicine, food, cosmetics, electronics and engineering. A review. *Environ Chem Lett* **18**, 851-869 (2020).
134. H. Luze, J. Holzer, I. B. de Mattos, A.-C. Tuca, S. P. Nischwitz, M. Funk, S. Mautner, T. Birngruber, L.-P. Kamolz, 526 Antiseptic Wound Dressings Made of Bacterial Nanocellulose. *Journal of burn care & research* **41**, S101-S101 (2020).
135. A. Resch, C. Staud, C. Radtke, Nanocellulose-based wound dressing for conservative wound management in children with second-degree burns. *Int Wound J* **18**, 478-486 (2021).
136. M. Bhattacharya, M. M. Malinen, P. Lauren, Y. R. Lou, S. W. Kuisma, L. Kanninen, M. Lille, A. Corlu, C. GuGuen-Guillouzo, O. Ikkala, A. Laukkanen, A. Urtti, M. Yliperttula, Nanofibrillar cellulose hydrogel promotes three-dimensional liver cell culture. *J Control Release* **164**, 291-298 (2012).
137. M. Colic, D. Mihajlovic, A. Mathew, N. Naseri, V. Kokol, Cytocompatibility and immunomodulatory properties of wood based nanofibrillated cellulose. *Cellulose* **22**, 763-778 (2015).
138. D. J. Modulevsky, C. M. Cuerrier, A. E. Pelling, Biocompatibility of Subcutaneously Implanted Plant-Derived Cellulose Biomaterials. *PLoS One* **11**, e0157894 (2016).

139. R. M. Domingues, M. E. Gomes, R. L. Reis, The potential of cellulose nanocrystals in tissue engineering strategies. *Biomacromolecules* **15**, 2327-2346 (2014).
140. R. J. Hickey, A. E. Pelling, Cellulose Biomaterials for Tissue Engineering. *Front Bioeng Biotechnol* **7**, 45 (2019).
141. H. R. Nordli, G. Chinga-Carrasco, A. M. Rokstad, B. Pukstad, Producing ultrapure wood cellulose nanofibrils and evaluating the cytotoxicity using human skin cells. *Carbohydr Polym* **150**, 65-73 (2016).
142. Y. R. Lou, L. Kanninen, T. Kuisma, J. Niklander, L. A. Noon, D. Burks, A. Urtti, M. Yliperttula, The use of nanofibrillar cellulose hydrogel as a flexible three-dimensional model to culture human pluripotent stem cells. *Stem Cells Dev* **23**, 380-392 (2014).
143. A. N. Leberfinger, D. J. Ravnic, A. Dhawan, I. T. Ozbolat, Concise Review: Bioprinting of Stem Cells for Transplantable Tissue Fabrication. *Stem Cells Transl Med* **6**, 1940-1948 (2017).
144. C. K. Arakawa, C. A. DeForest, in *Biology and Engineering of Stem Cell Niches,* A. Vishwakarma, J. M. Karp, Eds. (Academic Press, Boston, 2017), pp. 295-314.
145. A. Cooper, N. Bhattarai, M. Zhang, Fabrication and cellular compatibility of aligned chitosan–PCL fibers for nerve tissue regeneration. *Carbohyd Polym* **85**, 149-156 (2011).
146. C. Erisken, D. M. Kalyon, H. Wang, Functionally graded electrospun polycaprolactone and beta-tricalcium phosphate nanocomposites for tissue engineering applications. *Biomaterials* **29**, 4065-4073 (2008).
147. J. R. Porter, A. Henson, K. C. Popat, Biodegradable poly(epsilon-caprolactone) nanowires for bone tissue engineering applications. *Biomaterials* **30**, 780-788 (2009).
148. L. Shor, S. Güçeri, X. Wen, M. Gandhi, W. Sun, Fabrication of three-dimensional polycaprolactone/hydroxyapatite tissue scaffolds and osteoblast-scaffold interactions in vitro. *Biomaterials* **28**, 5291-5297 (2007).
149. H. Chi, A. Jiang, X. Wang, G. Chen, C. Song, R. K. Prajapati, A. Li, Z. Li, J. Li, Z. Zhang, Y. Ji, J. Yan, Dually optimized polycaprolactone/collagen I microfiber scaffolds with stem cell capture and differentiation-inducing abilities promote bone regeneration. *J Mater Chem B* **7**, 7052-7064 (2019).
150. Z. Izadifar, T. Chang, W. Kulyk, X. Chen, B. F. Eames, Analyzing Biological Performance of 3D-Printed, Cell-Impregnated Hybrid Constructs for Cartilage Tissue Engineering. *Tissue Eng Part C Methods* **22**, 173-188 (2016).
151. J. P. Armstrong, M. Burke, B. M. Carter, S. A. Davis, A. W. Perriman, 3D Bioprinting Using a Templated Porous Bioink. *Adv Healthc Mater*, (2016).
152. C. Ververis, K. Georghiou, N. Christodoulakis, P. Santas, R. Santas, Fiber dimensions, lignin and cellulose content of various plant materials

and their suitability for paper production. *Industrial Crops and Products* **19**, 245-254 (2004).
153. J. D. P. de Amorim, K. C. de Souza, C. R. Duarte, I. da Silva Duarte, F. de Assis Sales Ribeiro, G. S. Silva, P. M. A. de Farias, A. Stingl, A. F. S. Costa, G. M. Vinhas, L. A. Sarubbo, Plant and bacterial nanocellulose: production, properties and applications in medicine, food, cosmetics, electronics and engineering. A review. *Environ Chem Lett* **18**, 851-869 (2020).
154. H. Backdahl, G. Helenius, A. Bodin, U. Nannmark, B. R. Johansson, B. Risberg, P. Gatenholm, Mechanical properties of bacterial cellulose and interactions with smooth muscle cells. *Biomaterials* **27**, 2141-2149 (2006).
155. P. Gatenholm, J. Berry, A. Rojas, M. B. Sano, R. V. Davalos, K. Johnson, L. O'Rourke, Bacterial Nanocellulose Biomaterials with Controlled Architecture for Tissue Engineering Scaffolds and Customizable Implants. *Perspect Nanotechnol*, 197-216 (2013).
156. D. Klemm, F. Kramer, S. Moritz, T. Lindstrom, M. Ankerfors, D. Gray, A. Dorris, Nanocelluloses: a new family of nature-based materials. *Angew Chem Int Ed Engl* **50**, 5438-5466 (2011).
157. H. Martinez Avila, S. Schwarz, E. M. Feldmann, A. Mantas, A. von Bomhard, P. Gatenholm, N. Rotter, Biocompatibility evaluation of densified bacterial nanocellulose hydrogel as an implant material for auricular cartilage regeneration. *Appl Microbiol Biotechnol* **98**, 7423-7435 (2014).
158. L. Nimeskern, H. Martinez Avila, J. Sundberg, P. Gatenholm, R. Muller, K. S. Stok, Mechanical evaluation of bacterial nanocellulose as an implant material for ear cartilage replacement. *J Mech Behav Biomed Mater* **22**, 12-21 (2013).
159. J. Wu, Y. Zheng, W. Song, J. Luan, X. Wen, Z. Wu, X. Chen, Q. Wang, S. Guo, In situ synthesis of silver-nanoparticles/bacterial cellulose composites for slow-released antimicrobial wound dressing. *Carbohydr Polym* **102**, 762-771 (2014).
160. J. Wu, Y. Zheng, X. Wen, Q. Lin, X. Chen, Z. Wu, Silver nanoparticle/bacterial cellulose gel membranes for antibacterial wound dressing: investigation in vitro and in vivo. *Biomed Mater* **9**, 035005 (2014).
161. L. Brinchi, F. Cotana, E. Fortunati, J. M. Kenny, Production of nanocrystalline cellulose from lignocellulosic biomass: Technology and applications. *Carbohyd Polym* **94**, 154-169 (2013).
162. M. J. Dunlop, B. Acharya, R. Bissessur, Study of plant and tunicate based nanocrystalline cellulose in hybrid polymeric nanocomposites. *Cellulose* **27**, 249-261 (2020).
163. P. S. Belton, S. F. Tanner, N. Cartier, H. Chanzy, High-Resolution Solid-State C-13 Nuclear Magnetic-Resonance Spectroscopy of Tunicin, an Animal Cellulose. *Macromolecules* **22**, 1615-1617 (1989).

164. S. Kimura, T. Itoh, New cellulose synthesizing complexes (terminal complexes) involved in animal cellulose biosynthesis in the tunicate Metandrocarpa uedai. *Protoplasma* **194**, 151-163 (1996).
165. H. W. Kang, S. J. Lee, I. K. Ko, C. Kengla, J. J. Yoo, A. Atala, A 3D bioprinting system to produce human-scale tissue constructs with structural integrity. *Nat Biotechnol* **34**, 312-319 (2016).
166. J. Malda, J. Visser, F. P. Melchels, T. Jungst, W. E. Hennink, W. J. Dhert, J. Groll, D. W. Hutmacher, 25th anniversary article: Engineering hydrogels for biofabrication. *Adv Mater* **25**, 5011-5028 (2013).
167. A. N. Leberfinger, S. Dinda, Y. Wu, S. V. Koduru, V. Ozbolat, D. J. Ravnic, I. T. Ozbolat, Bioprinting functional tissues. *Acta Biomater* **95**, 32-49 (2019).
168. A. B. Dababneh, I. T. Ozbolat, Bioprinting Technology: A Current State-of-the-Art Review. *J Manuf Sci E-T Asme* **136**, (2014).
169. B. Duan, L. A. Hockaday, K. H. Kang, J. T. Butcher, 3D bioprinting of heterogeneous aortic valve conduits with alginate/gelatin hydrogels. *J Biomed Mater Res A* **101**, 1255-1264 (2013).
170. K. Nair, M. Gandhi, S. Khalil, K. C. Yan, M. Marcolongo, K. Barbee, W. Sun, Characterization of cell viability during bioprinting processes. *Biotechnol J* **4**, 1168-1177 (2009).
171. M. Castilho, R. Levato, P. N. Bernal, M. de Ruijter, C. Y. Sheng, J. van Duijn, S. Piluso, K. Ito, J. Malda, Hydrogel-Based Bioinks for Cell Electrowriting of Well-Organized Living Structures with Micrometer-Scale Resolution. *Biomacromolecules* **22**, 855-866 (2021).
172. B. K. Gu, D. J. Choi, S. J. Park, M. S. Kim, C. M. Kang, C.-H. Kim, 3-dimensional bioprinting for tissue engineering applications. *Biomaterials Research* **20**, 12 (2016).
173. A. Aung, G. Gupta, G. Majid, S. Varghese, Osteoarthritic chondrocyte-secreted morphogens induce chondrogenic differentiation of human mesenchymal stem cells. *Arthritis Rheum* **63**, 148-158 (2011).
174. E. Grimaud, D. Heymann, F. Redini, Recent advances in TGF-beta effects on chondrocyte metabolism. Potential therapeutic roles of TGF-beta in cartilage disorders. *Cytokine Growth Factor Rev* **13**, 241-257 (2002).
175. V. Lettry, K. Hosoya, S. Takagi, M. Okumura, Coculture of equine mesenchymal stem cells and mature equine articular chondrocytes results in improved chondrogenic differentiation of the stem cells. *Jpn J Vet Res* **58**, 5-15 (2010).
176. L. Wu, J. Leijten, C. A. van Blitterswijk, M. Karperien, Fibroblast growth factor-1 is a mesenchymal stromal cell-secreted factor stimulating proliferation of osteoarthritic chondrocytes in co-culture. *Stem Cells Dev* **22**, 2356-2367 (2013).
177. L. Wu, J. C. Leijten, N. Georgi, J. N. Post, C. A. van Blitterswijk, M. Karperien, Trophic effects of mesenchymal stem cells increase chondrocyte proliferation and matrix formation. *Tissue Eng Part A* **17**, 1425-1436 (2011).

178. J. L. Jones, A. M. Hanby, C. Wells, M. Calaminici, L. Johnson, P. Turton, R. Deb, E. Provenzano, A. Shaaban, I. O. Ellis, S. E. Pinder, Breast implant-associated anaplastic large cell lymphoma (BIA-ALCL): an overview of presentation and pathogenesis and guidelines for pathological diagnosis and management. *Histopathology* **75**, 787-796 (2019).
179. W. Jia, P. S. Gungor-Ozkerim, Y. S. Zhang, K. Yue, K. Zhu, W. Liu, Q. Pi, B. Byambaa, M. R. Dokmeci, S. R. Shin, A. Khademhosseini, Direct 3D bioprinting of perfusable vascular constructs using a blend bioink. *Biomaterials* **106**, 58-68 (2016).
180. Y.-D. Zhao, J.-H. Lai, M. Wang, 4D Printing of Self-Folding Hydrogel Tubes for Potential Tissue Engineering Applications. *Nano LIFE* **11**, 2141001 (2021).
181. A. J. Seymour, S. Shin, S. C. Heilshorn, 3D Printing of Microgel Scaffolds with Tunable Void Fraction to Promote Cell Infiltration. *Advanced healthcare materials* **10**, 2100644-n/a (2021).
182. L. Shao, Q. Gao, C. Xie, J. Fu, M. Xiang, Z. Liu, L. Xiang, Y. He, Sacrificial microgel-laden bioink-enabled 3D bioprinting of mesoscale pore networks. *Bio-design and manufacturing* **3**, 30-39 (2020).
183. T. Möller, M. Amoroso, D. Hägg, C. Brantsing, N. Rotter, P. Apelgren, A. Lindahl, L. Kölby, P. Gatenholm, In Vivo Chondrogenesis in 3D Bioprinted Human Cell-laden Hydrogel Constructs. *Plastic and Reconstructive Surgery - Global Open* **5**, (2017).
184. O. Jalnefjord, M. Andersson, M. Montelius, G. Starck, A. K. Elf, V. Johanson, J. Svensson, M. Ljungberg, Comparison of methods for estimation of the intravoxel incoherent motion (IVIM) diffusion coefficient (D) and perfusion fraction (f). *MAGMA* **31**, 715-723 (2018).
185. V. N. Anisimov, [Life span and tumor incidence in animals of various species]. *Eksp Onkol* **9**, 17-23, 60 (1987).
186. V. N. Anisimov, M. A. Zabezhinski, G. Rossolini, A. Zaia, A. Piantanelli, A. Basso, L. Piantanelli, Long-live euthymic BALB/c-nu mice. II: spontaneous tumors and other pathologies. *Mech Ageing Dev* **122**, 477-489 (2001).
187. L. Piantanelli, A. Zaia, G. Rossolini, A. Piantanelli, A. Basso, V. N. Anisimov, Long-live euthymic BALB/c-nu mice. I. Survival study suggests body weight as a life span predictor. *Mech Ageing Dev* **122**, 463-475 (2001).
188. G. Siegel, T. Kluba, U. Hermanutz-Klein, K. Bieback, H. Northoff, R. Schafer, Phenotype, donor age and gender affect function of human bone marrow-derived mesenchymal stromal cells. *BMC Med* **11**, 146 (2013).
189. J. Garcia, C. Mennan, H. S. McCarthy, S. Roberts, J. B. Richardson, K. T. Wright, Chondrogenic Potency Analyses of Donor-Matched Chondrocytes and Mesenchymal Stem Cells Derived from Bone Marrow, Infrapatellar Fat Pad, and Subcutaneous Fat. *Stem Cells Int* **2016**, 6969726 (2016).

190. B. Arzi, G. D. DuRaine, C. A. Lee, D. J. Huey, D. L. Borjesson, B. G. Murphy, J. C. Y. Hu, N. Baumgarth, K. A. Athanasiou, Cartilage immunoprivilege depends on donor source and lesion location. *Acta Biomater* **23**, 72-81 (2015).
191. R. Domenis, L. Lazzaro, S. Calabrese, D. Mangoni, A. Gallelli, E. Bourkoula, I. Manini, N. Bergamin, B. Toffoletto, C. A. Beltrami, A. P. Beltrami, D. Cesselli, P. C. Parodi, Adipose tissue derived stem cells: in vitro and in vivo analysis of a standard and three commercially available cell-assisted lipotransfer techniques. *Stem cell research & therapy* **6**, 2-2 (2015).
192. B. T. Estes, B. O. Diekman, J. M. Gimble, F. Guilak, Isolation of adipose-derived stem cells and their induction to a chondrogenic phenotype. *Nat Protoc* **5**, 1294-1311 (2010).
193. A. Sterodimas, J. de Faria, B. Nicaretta, I. Pitanguy, Tissue engineering with adipose-derived stem cells (ADSCs): current and future applications. *J Plast Reconstr Aesthet Surg* **63**, 1886-1892 (2010).
194. Y. Zhao, S. D. Waldman, L. E. Flynn, Multilineage co-culture of adipose-derived stem cells for tissue engineering. *J Tissue Eng Regen Med* **9**, 826-837 (2015).